

Sensorless Technique for BLDC Motors

by

Daniele Gambetta, B.Sc (Hons)

Dissertation

Submitted in Fulfillment

of the Requirements

for the Degree of

Master of Philosophy

at the

The University of Southern Queensland

Faculty of Engineering & Surveying

February 2006

Copyright
by
Daniele Gambetta
2006

Abstract

Commutation is a fundamental feature of all DC machines. In conventional DC machines the commutation function is performed by the commutator and brushes. These act as both position sensors and switches. The mechanical commutator has obvious disadvantages. Overcoming those disadvantages has been a major reason behind the development of brushless DC (BLDC) machines. In brushless DC machines commutation is performed by power electronic devices forming part of an inverter bridge. However, switching of the power electronic devices has to be synchronised with rotor position. Position sensing is therefore an essential requirement. This can be done by using sensors such as Hall Effect devices or a sensorless approach may be adopted. Advantages of sensorless techniques include reduced cost and wiring. The most common sensorless method is based on detection of the zero crossing of back EMF signals. But this technique works only above a certain speed since back EMF is directly proportional to speed. As a result BLDC systems which rely solely on back EMF signals for commutation suffer from

relatively poor starting performance characterised by back rotation of up to one hundred and eighty electrical degrees and large fluctuations in electromagnetic torque resulting from non-ideal commutation instants. This may not be acceptable for some applications and many researchers have attempted to overcome those problems. The aim of this project has been to investigate the possibility of a sensorless technique which does not cost more than the back EMF method but with a performance at start-up comparable with that obtained when Hall sensors are used. Initial investigations led to a saliency based method. Detailed theoretical analysis is presented which shows that the method is insensitive to variations in operational parameters such as load current and circuit parameters such as power device voltage drops and winding resistances. There is a close parallel between it and the back EMF method and this makes it easy to swap to the latter method at high speed if necessary. A starting strategy, relying on saliency related measurements, is proposed which offers starting performance much better than the back EMF method and almost as good as Hall sensor based techniques. Experimental evidence is provided to confirm that commutation instants determined by the proposed method are practically coincident with those obtained when Hall sensors are used.

Certification of Thesis

I certify that the ideas, experimental work, results, analyses, software and conclusions reported in this dissertation are entirely my effort, except where otherwise acknowledged. I also certify that the work is original and has not been previously submitted for any other award, expect where otherwise acknowledged.



Signature of Candidate

Date

ENDORSEMENT

Signature of Supervisors

Date

Acknowledgments

I would sincerely like to thank and acknowledge the following people for their assistance, guidance and support throughout the duration of this project.

First of all I would like to thank my supervisor Dr Tony Ahfock. This study would not have been possible without his continued guidance, support and advice. Throughout the duration of this project he has been extremely patient, inspiring and has been a pleasure to work with.

I am also very grateful to Mr Aspesi (CEO of the funding company, Metallux SA) for his continued support, interest in and assistance with the project.

I wish to thank the Faculty of Engineering and Surveying and the Office of Research and Higher Degrees for their support and assistance. My thanks also extends to all those at the University who made this such a pleasant experience.

Finally, I wish to thank my family for their continued support and encouragement.

Contents

ABSTRACT	III
CERTIFICATION OF THESIS	V
ACKNOWLEDGMENTS	VI
CONTENTS	VIII
LIST OF TABLES	XII
LIST OF FIGURES	XIV
CHAPTER 1 INTRODUCTION	1
1.1 THE BRUSHLESS DC (BLDC) MOTOR.....	1
1.2 PERFORMANCE CHARACTERISTICS.....	5
1.2.1 <i>Speed Control Performance</i>	5

1.2.2	<i>Performance During Start-up</i>	8
1.3	PROJECT OBJECTIVES	14
1.4	OUTLINE OF THE DISSERTATION	15
CHAPTER 2 LITERATURE REVIEW		16
2.1	INTRODUCTION.....	16
2.2	SATURATION BASED METHODS	17
2.3	METHODS BASED ON ROTOR INHERENT SALIENCY	21
2.4	BACK EMF BASED METHODS	22
2.5	CONCLUSIONS	24
CHAPTER 3 PRELIMINARY INVESTIGATIONS		26
3.1	PURPOSE OF INVESTIGATIONS.....	26
3.2	THE TEST MACHINE	27
3.3	INVERTER BRIDGE OPERATION.....	29
3.3.1	<i>Unipolar Switching</i>	30
3.3.2	<i>Bipolar Switching</i>	31
3.4	PULSE INJECTION	33
3.5	STAR-POINT VOLTAGE RESPONSE	35
3.6	THE SELECTED METHOD	38
CHAPTER 4 THE EQUAL INDUCTANCE METHOD		39
4.1	INTRODUCTION.....	39
4.2	MATHEMATICAL MODEL	40

4.3	RELATIONSHIP BETWEEN IDEAL COMMUTATION POSITIONS AND EQUAL INDUCTANCE POSITIONS.....	45
4.4	DETECTING EQUAL SELF-INDUCTANCE POSITIONS.....	47
4.5	SENSITIVITY OF THE PROPOSED POSITION SENSING METHOD.....	53
4.6	DETECTION OF ROTOR INITIAL POSITION	57
4.7	TRANSFER TO OR FROM THE BACK EMF METHOD	60
CHAPTER 5 PRACTICAL IMPLEMENTATION		63
5.1	INTRODUCTION.....	63
5.2	HARDWARE DESCRIPTION	65
5.2.1	<i>Overview</i>	<i>65</i>
5.2.2	<i>The Control Module.....</i>	<i>66</i>
5.2.3	<i>The selected DSC.....</i>	<i>67</i>
5.2.4	<i>The H-bridge.....</i>	<i>67</i>
5.3	LAYOUT AND PCB MANUFACTURING	69
5.4	SOFTWARE DESCRIPTION	70
5.4.1	<i>Overview</i>	<i>70</i>
5.4.2	<i>Program structure.....</i>	<i>71</i>
5.4.3	<i>The 'Run' state.....</i>	<i>72</i>
5.4.4	<i>The start-up process.....</i>	<i>84</i>
5.5	TEST RESULTS.....	86
CHAPTER 6 CONCLUSIONS.....		89
6.1	THEORETICAL FINDINGS	89

6.2	PRACTICAL OUTCOME.....	92
6.3	FURTHER WORK.....	93
	REFERENCES.....	95
	APPENDIX A FIRMWARE	99

List of Tables

TABLE 1.1 : BLDC MOTOR CONTROL SYSTEMS: PERFORMANCE CHARACTERISTICS	8
TABLE 1.2 : ROTOR POSITION INDICATION	12
TABLE 3.1 : MAGNETIC PROPERTIES OF THE CM120 MOTOR MAGNETS (SOURCE: BOMATEC AG)	27
TABLE 3.2 : PHYSICAL AND MECHANICAL PROPERTIES OF THE CM120 MOTOR MAGNETS (SOURCE: BOMATEC LTD).....	27
TABLE 3.3 : TEST MOTOR NAMEPLATE DATA	28
TABLE 3.4 : MEASURED STAR POINT VOLTAGE WAVEFORMS	37
TABLE 4.1 : ANGULAR POSITIONS AT WHICH SELF INDUCTANCES ARE EQUAL	46
TABLE 4.2 : COMPARISON BETWEEN COMMUTATION POSITIONS AND POSITIONS AT WHICH SELF- INDUCTANCES ARE EQUAL	46
TABLE 4.3 : LOOK-UP TABLE FOR DETECTION OF INITIAL ROTOR POSITION	59

TABLE 5.1 : COMPARISON OF MOTOR CURRENT (DC) AND SPEED FOR GIVEN PWM DUTY RATIOS

..... 86

List of Figures

FIGURE 1.1 : BLDC ROTORS WITH SURFACE MAGNETS (SOURCE: MILLER 1989).....	2
FIGURE 1.2 : BLDC ROTORS WITH INTERNAL MAGNETS (SOURCE: MILLER 1989)	2
FIGURE 1.3 : INVERTER FED BLDC STATOR WINDINGS	3
FIGURE 1.4 : IDEALISED CURRENTS SUPPLIED BY INVERTER	4
FIGURE 1.5 : BLOCK DIAGRAM OF TYPICAL BLDC MOTOR DRIVE INCORPORATING CLOSED LOOP SPEED CONTROL	5
FIGURE 1.6 : COMMUTATION STATES AND ROTOR POSITION (θ)	9
FIGURE 1.7 : COMMUTATION STATES AND ROTOR START-UP POSITION.....	10
FIGURE 2.1 : ROTOR FLUX AFFECTING FLUX PRODUCED BY PHASE WINDING (SOURCE: SCHMIDT ET AL., 1997)	18
FIGURE 2.2 : STATOR INDUCTANCE AS A FUNCTION OF ROTOR POSITION (SOURCE: SCHMIDT ET AL., 1997).....	19

FIGURE 2.3 : INDUCTANCE VARIATION DUE TO SATURATION (SOURCE: CHIRICOZZI ET AL.,1998)	20
.....	20
FIGURE 2.4 : CURRENT DIFFERENCES (SOURCE: CHIRICOZZI ET AL.,1998)	20
FIGURE 3.1 : ROTOR OF THE CM120 MACHINE (SOURCE: ELTRONIC LTD)	28
FIGURE 3.2 : THREE PHASE BRIDGE INVERTER CONNECTED TO BLDC	29
FIGURE 3.3 : UNIPOLAR SWITCHING STRATEGY (CHALUPA, 2001)	31
FIGURE 3.4 : BIPOLAR SWITCHING STRATEGY (CHALUPA, 2001)	32
FIGURE 3.5 : D- AND Q-AXIS STEP RESPONSE (IN ALIGNMENT WITH PHASE A)	34
FIGURE 3.6 : STAR-POINT VOLTAGE WAVEFORM	36
FIGURE 4.1 : MEASURED SELF-INDUCTANCES	41
FIGURE 4.2 : MEASURED MUTUAL-INDUCTANCES	42
FIGURE 4.3 : IDEALIZED BACK EMF WAVEFORMS	43
FIGURE 4.5 : COMMUTATION ALGORITHM	47
FIGURE 4.6 : INVERTER BRIDGE SUPPLYING A BRUSHLESS DC MOTOR	47
FIGURE 4.7 : THE TWELVE POSSIBLE INVERTER STATES	49
FIGURE 4.8 : EQUIVALENT CIRCUITS FOR INVERTER STATES A^+B^- AND B^+A^-	50
FIGURE 4.9 : ALGORITHM FOR ROTOR INITIAL POSITION DETECTION ⁻	58
FIGURE 4.10 : TRANSFER TO OR FROM THE BACK EMF METHOD ⁻	61
FIGURE 4.11 : CHANGE OF STATE OF EL FLAG WITH SPEED	62
FIGURE 5.1 : OVERALL SYSTEM MODEL	64
FIGURE 5.2 : HARDWARE BLOCK DIAGRAM	65
FIGURE 5.3 : THE CONTROL MODULE	66
FIGURE 5.4 : MOSFET AND SHUNT CONNECTIONS	68

FIGURE 5.5 : BOTTOM-LAYER OF THE CONTROL MODULE	69
FIGURE 5.6 : THE DRIVE (CONTROL MODULE AND POWER SEMICONDUCTORS).....	69
FIGURE 5.7 : STATE TRANSITION DIAGRAM	70
FIGURE 5.8 : MAIN PROGRAM	71
FIGURE 5.9 : PWM RELOAD ISR	73
FIGURE 5.10 : SYNCHRONISATION OF PWM RELOAD ISR	73
FIGURE 5.11 : ADC COMPLETE ISR	75
FIGURE 5.12 : FLOW CHART FOR THE ADC COMPLETE ISR (PART1)	76
FIGURE 5.13 : FLOW CHART FOR THE ADC COMPLETE ISR (PART 2).....	77
FIGURE 5.14 : DEFINITION OF PARAMETERS USED IN ADC COMPLETE ISR	78
FIGURE 5.15 : COMMUTATION TIMER (QTC0) OC ISR	79
FIGURE 5.16 : FLOW CHART FOR THE COMMUTATION TIMER (QTC0) OC ISR	80
FIGURE 5.17 : TIMING DIAGRAM SHOWING OPERATION OF THE COMMUTATION TIMER	81
FIGURE 5.18 : SPEED TIMER ISR.....	83
FIGURE 5.19 : START/STOP REQUEST ISR	83
FIGURE 5.20 : START-UP TIMER ISR	85
FIGURE 5.21A : COMPARISON OF THE COMMUTATION INSTANT (DETAIL).....	87
FIGURE 5.21B : COMPARISON OF THE COMMUTATION INSTANTS (AT NO LOAD, 100MA).....	88
FIGURE 5.21C : COMPARISON OF THE COMMUTATION INSTANTS (AT 500 MA)	88

Chapter 1

Introduction

1.1 The Brushless DC (BLDC) Motor

Fundamentally the brushless DC (BLDC) motor is very similar to the classical separately excited DC motor. Excitation for the latter is provided by windings or permanent magnets mounted on the stator. In the BLDC motor excitation is provided by permanent magnets mounted on the rotor. Figures 1.1 and 1.2 show a number of methods used to mount the magnets on the rotor. There has been remarkable progress made in the development of high quality magnets in the last few decades. At present high performance NdFeB (neodymium-iron-boron) (Krishnan, 2001) magnets are widely used in BLDC motors.

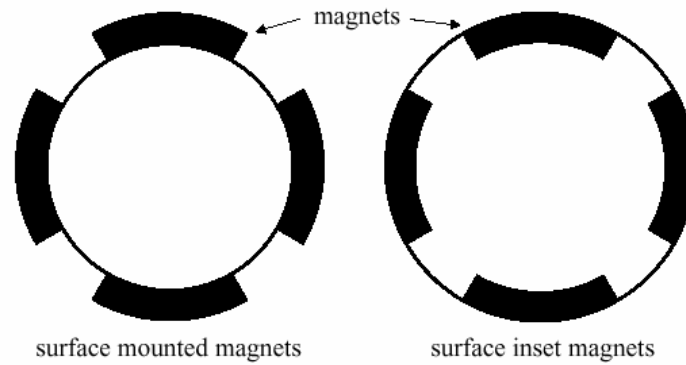
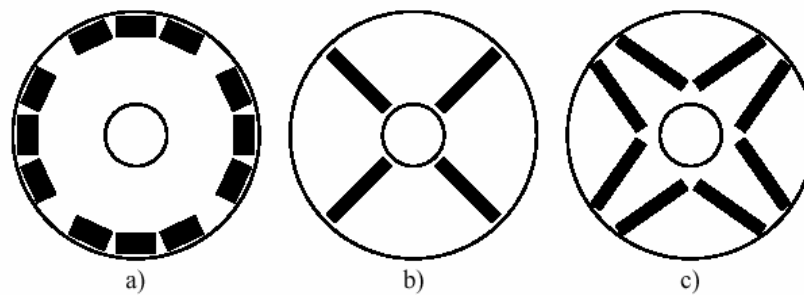


Figure 1.1 : BLDC rotors with surface magnets (Source: Miller 1989)

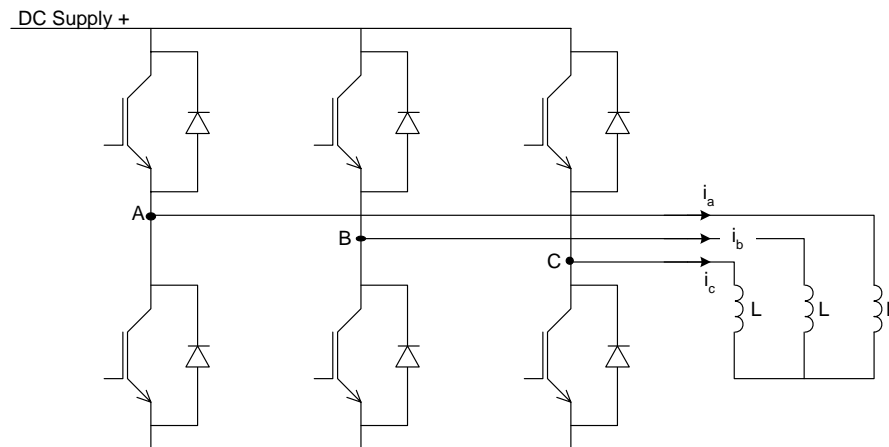


a) Surface buried,
b) radial, and c) v-arranged magnets (black areas are the magnets)

Figure 1.2 : BLDC rotors with Internal Magnets (Source: Miller 1989)

Reversal of direction of coil currents at precise rotor positions is essential in both conventional DC motors and in BLDC motors. In conventional motors this is carried out by means of the shaft mounted mechanical commutator and the brushes. The commutator and brushes act both as a set of switches to carry out current reversal and as a position sensor which ensures that the reversals are initiated at the right instants. In the BLDC motor electrical energy is fed to coils residing on

the stator and as mentioned before excitation is provided by rotor mounted permanent magnets. Therefore there is no requirement for brushes and this is the most important advantage of BLDC motors compared to classical DC motors. There is still a requirement for stator coil current reversals to be synchronized with appropriate rotor positions. As in the case of the classical DC motor, this involves switching and position sensing. In the BLDC motor, however, switching and position detection are done separately. Switching is performed by power semiconductors, typically in a three-phase inverter bridge configuration using MOSFETs or IGBTs (see Figure 1.3). This implies that BLDC motors are normally three-phase wound with each motor line current controlled by one leg of the three-phase bridge. The inverter is operated in PWM mode with two out of the three-phase windings energized at any one time (Valentine, 1998). Figure 1.4 displays idealized phase currents supplied by the inverter. Note that ideally there are six commutation states in one cycle of operation. These have been labeled CB, AB, AC, BC, BA and CA.



Note : 3-phase windings assumed star connected, some BLDC motors are delta connected.

Figure 1.3 : Inverter fed BLDC stator windings

Phase current reversals have to be initiated at rotor angular positions θ_1 , θ_2 , θ_3 , θ_4 , θ_5 , and θ_6 . The rotor position detection technique has to be carefully selected for each application taking into consideration factors such as performance requirements, cost, available space envelope and the physical environment.

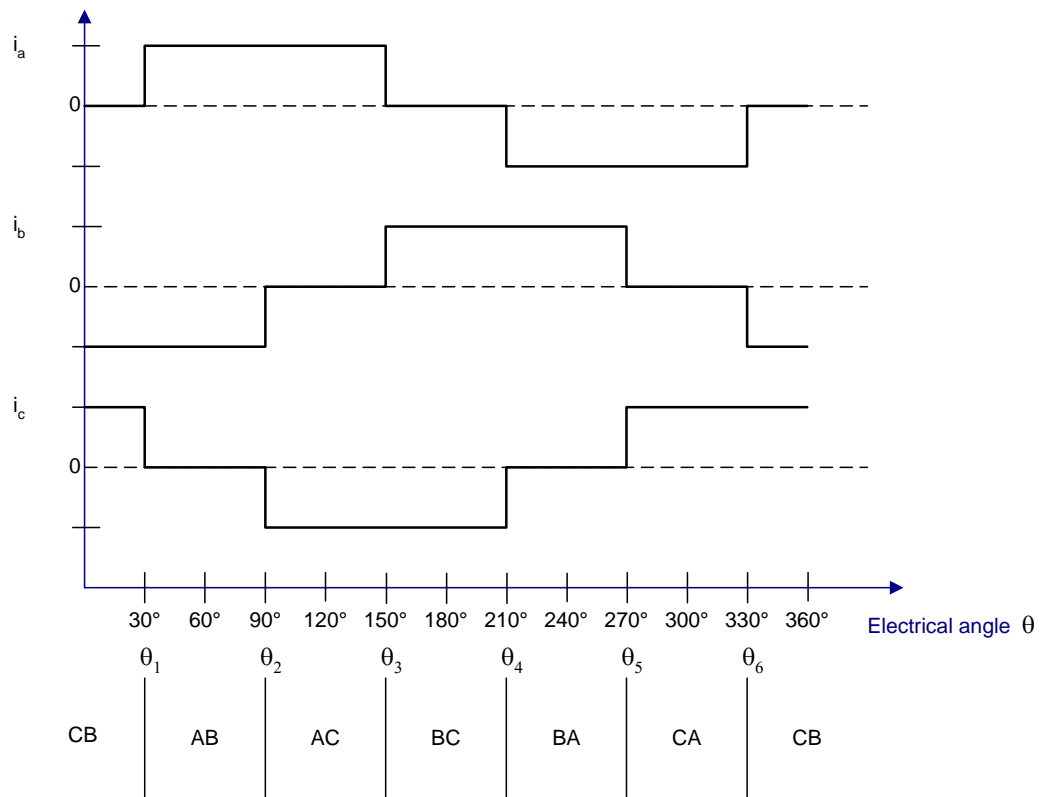


Figure 1.4 : Idealised currents supplied by Inverter

1.2 Performance Characteristics

1.2.1 Speed Control Performance

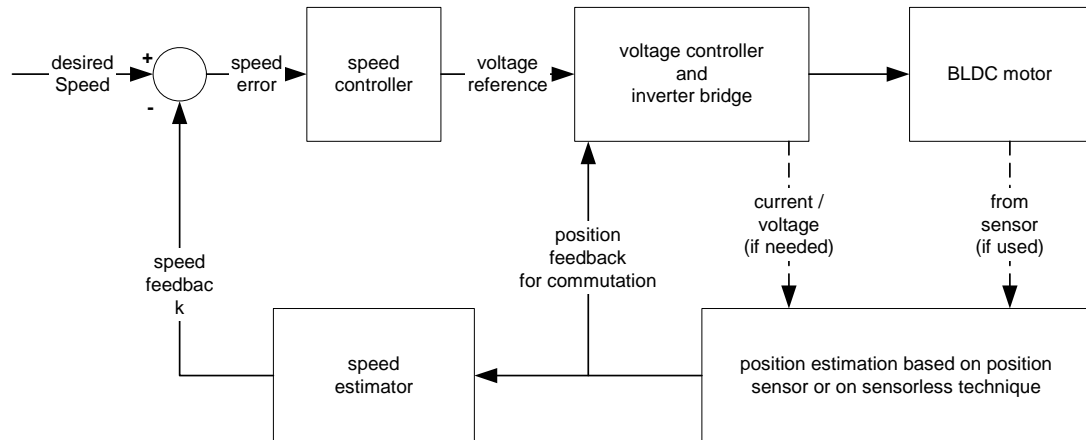


Figure 1.5 : Block diagram of typical BLDC motor drive incorporating closed loop speed control

It has already been pointed out that position detection, in BLDC motor control, has the primary role of initiating commutation or current reversal in the armature windings. Very often, however, closed loop control of speed is a practical requirement. In such cases position information is also used for speed estimation. Figure 1.5 is a block diagram of a typical BLDC drive system incorporating closed loop speed control. The feedback loop for commutation is shown. A current control loop is sometimes implemented in addition to or instead of the voltage control loop. In Figure 1.5, this has not been shown explicitly, but it is within the voltage controller block. Operating details of each loop will be provided in later chapters. The basic principle, however, is

such that a speed error causes the voltage or current reference to change in the appropriate direction (rise or fall). The voltage controller, in turn, raises or lowers the applied motor voltage. This results in a change of electromagnetic (or driving) force which, if the speed control loop is well-designed, will correct the speed until the speed error returns to zero.

The performance of BLDC motors, especially near standstill and during start-up, depends critically on the nature of the available position information. Table 1.1 provides a summary of typical performance characteristics of systems that are readily available commercially. A high resolution shaft encoder would offer the best performance over the entire speed range, from standstill to rated speed. The fundamental reasons for this are that the encoder can give absolute rotor position at any speed and that the resolution is high enough for speed to be accurately determined by differentiation. The high resolution encoder, however, increases significantly the overall system cost and it is used only when there is strong justification for doing so.

Low resolution position sensors such as Hall sensors provide reasonable compromise between performance and cost. Signals from the sensors provide accurate commutation instants for the inverter at any speed. It is not possible, however, to make accurate estimation of low speeds because of the excessive time between successive changes of state of sensor outputs. For this reason closed loop speed control is normally suppressed at low speed. But, in many applications this is not a problem because precise speed control at low speed is not a requirement.

The system cost can be reduced even further if physical position sensors are completely eliminated. The most popular sensorless method is based on the detection of the zero crossings

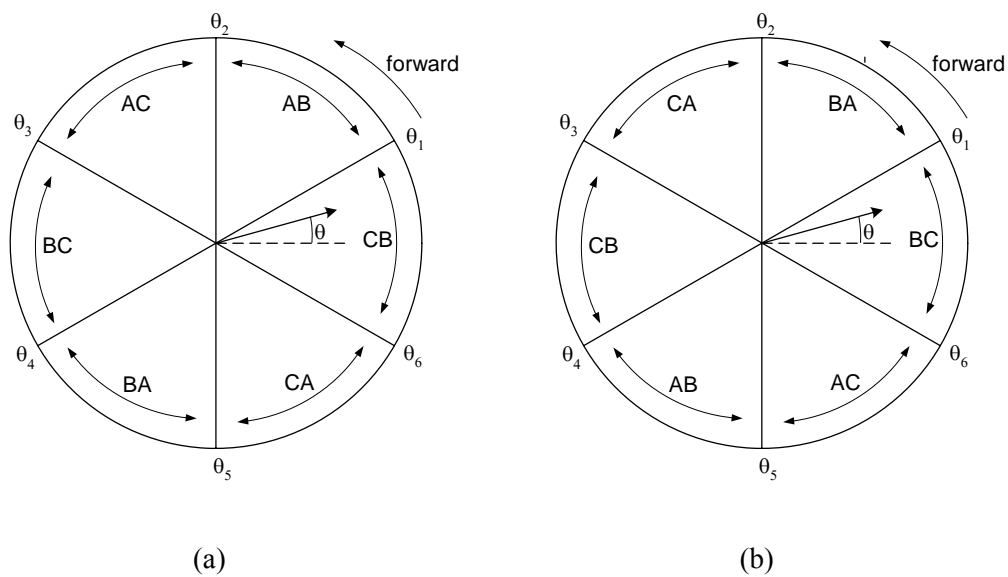
of back EMF signals. As will be shown later, there is normally a simple relationship between the instant of a zero crossing and the next desirable commutation instant. The zero crossing instants of the back EMF signals are also used to estimate speed. But, in common with the technique based on Hall sensors, accurate speed estimation at low speeds is not possible. However, unlike Hall sensors which provide position information at any speed, the back EMF technique is useless at low speeds because back EMF signals become excessively low. At low speeds and during start-up BLDC motor drives using the back EMF technique have to operate under open-loop speed control and without the position information required to help with commutation. Performance during start-up when Hall sensors are used is therefore better compared to performance with the back EMF technique.

1.2.2 Performance During Start-up

Table 1.1 : BLDC motor control systems: performance characteristics

Source of position information	Speed control performance	Start-Up performance	Relative cost
high resolution shaft encoder	excellent throughout speed range from standstill to rated speed	alignment stage not needed (if an absolute encoder is used); Guaranteed absence of back-rotation at start-up; smooth start-up	high; needs additional space and wiring
low resolution sensor; example: Hall sensor	good closed loop performance at speeds typically higher than 5% of rated value; closed loop operation not possible below that speed	alignment stage not needed; Guaranteed absence of back-rotation at start-up; smooth start-up	medium; needs wiring to connect to sensors
sensorless: back EMF	good closed loop performance at speeds typically higher than 5% of rated value; closed loop operation not possible below that speed	needs alignment stage before start-up; Cannot guarantee absence of initial back-rotation hard to ensure smooth start-up	low

Consider a BLDC motor that is rotating under normal operation. The position of the rotor, represented by θ in Figure 1.6, would increase with time in the positive direction for forward rotation or in the negative direction for reverse rotation. The inverter is normally controlled in such a way that the idealized current supply to the motor can be in one of six possible states (so called six step control technique).



Note:

With initial rotor position is as shown in (a) forward rotation is achieved by inverter states

CB,AB,AC,BC,BA,CA,CB...

With initial rotor position is as shown in (b) reverse rotation is achieved by inverter states

BC,AC,AB,CB,CA,BA,BC...

Figure 1.6 : Commutation states and rotor position (θ)

The states have been labeled CB, AB, AC, BC, BA and CA in accordance with Figure 1.4. For clarity separate diagrams have been used to illustrate forward and reverse rotation. It is assumed that when θ lies between -30 and 30 electrical degrees, state AB results in forward driving torque. This implies that under the same conditions, state BA results in reverse driving torque. Under normal operation, if forward rotation (anti-clockwise) is desired, then commutation of the inverter will be such that it goes into states CB, AB, AC, BC, BA and CA in cyclic order. This can be deduced from Figure 1.6(a). On the other hand, if reverse (clockwise) rotation is needed, the commutation states should go cyclically through states BC, AC, AB, CB, CA and BA. This can be deduced from Figure 1.6(b). Commutation should take place at rotor positions θ_1 , θ_2 , θ_3 , θ_4 , θ_5 , and θ_6 . These are marked in Figure 1.6.

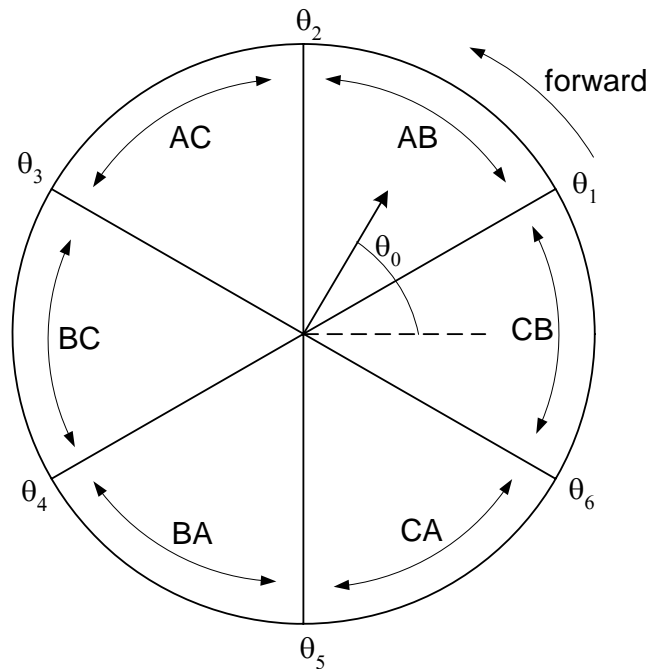


Figure 1.7 : Commutation states and rotor start-up position

Now consider a BLDC motor that is stationary, with its rotor position equal to θ_0 as shown in Figure 1.7. The motor needs to be started in forward direction. In practice θ_0 could be anywhere between 0 and 360 electrical degrees. However to help present the forthcoming arguments, it has been assumed that it is somewhere between 30 and 90 electrical degrees. If θ_0 is known, as would be the case if a high resolution absolute encoder is being used, there are no starting problems. There is enough information to decide on an appropriate starting state as well as subsequent commutation instants. In the chosen case, the first commutation state will be AB followed by AC (Figure 1.7). If Hall sensors are being used instead of a shaft encoder, then, generally, the information on θ_0 is limited. Only the 60 degree range in which θ_0 falls may be deduced from the Hall sensor signals (Table 1.2). Fortunately that limited information is sufficient to decide on the first inverter state. Therefore start-up with Hall sensors is as straightforward as with high resolution shaft encoders, except in the latter case closed loop speed control is possible down to standstill. As pointed out before, the resolution of Hall sensors, does not allow instantaneous speed to be estimated quickly and accurately enough for the purpose of closed loop feedback at low speed. Hence, at the lower end of the speed range, start-up is carried out under open-loop. On the other hand Hall sensors allow smooth start-up because they generate high quality position signals for commutation purposes down to the lowest speeds including standstill.

Table 1.2 : Rotor Position Indication

(Hall Sensors located in appropriate locations 120 electrical degrees apart)

Output State of Hall sensor A	Output state of Hall Sensor B	Output State of Hall Sensor C	Range in which rotor position θ falls
1	0	0	θ_1 to θ_2
1	1	0	θ_2 to θ_3
0	1	0	θ_3 to θ_4
0	1	1	θ_4 to θ_5
0	0	1	θ_5 to θ_6
1	0	1	θ_6 to θ_1

Starting is more difficult with the sensorless technique based on back EMF zero crossings. The fundamental reason for this is that at standstill there is no back EMF and therefore no position information. In other words, the value of θ_0 , the starting rotor position in Figure 1.7, is completely unknown. Typically, an alignment stage is used to get around the problem. This requires a predefined first commutation state chosen independently of initial rotor position. The first state could be any one of the possible six shown in Figure 1.7. A different but known alignment angle is associated with each state. For example if alignment is carried out using state AB, rotor alignment will occur at θ_3 , irrespective of the initial rotor position. Similarly if alignment is carried out using inverter state CA rotor alignment will occur at θ_1 . It should be obvious that there is no particular advantage in choosing any one of the six commutation state over any other for the alignment stage. Note that the alignment stage may cause back-rotation of up to 180 electrical degrees. For example if inverter state CB is chosen for alignment and θ_0 was initially equal to 10 degrees, then alignment is achieved by a forward rotation of 80 degrees. On

the other hand if θ_0 happened to be 269 degrees, then alignment is achieved by mean of a backward rotation of 179 degrees. This can be deduced by using Figure 1.7. Depending on which inverter state is used, the assumed rotor alignment position will be θ_1 , or θ_2 , or θ_3 and so on. The challenge for system designers is to estimate the time taken for the alignment stage to be completed. If it can be ascertained that alignment has been achieved, it is easy to decide which inverter state should be the next one. For example if inverter state CB was used for alignment, then for forward rotation, the first inverter state after alignment should be AC followed by BC, BA and so on. Apart from the disadvantages of requiring an alignment stage and the real possibility of back-rotation during alignment, the back EMF method suffers another disadvantage because initially, when speed is still low, there is no way of detecting commutation positions θ_1 , θ_2 , θ_3 and so on. Designers can only organize commutation based on estimates of rotor position with time. Actual rotor position at a particular time depends on many factors such as speed, moment of inertia of the motor-load combination, non-inertial load torque on the motor including friction and electrical quantities such as voltage and current. Estimation of rotor position is very likely to be difficult, yet performance during start up depends heavily of good estimates of it. Therefore it is hard to guarantee smooth start-up specially if there are variations in operating conditions.

A summary of start-up performance characteristics of BLDC motor drive systems that are commercially available is given in Table 1.1.

1.3 Project Objectives

The sensorless technique based on the detection of zero crossings of back EMF signals has definite advantages of reduced cost, reduced wiring requirements, better suitability to harsh physical environment and reduced demand on space requirements. But it also has some drawbacks, specially during start-up and at low speeds. While these may be tolerated in some applications, there would be other applications for which the back EMF technique would not be considered because of its disadvantages. There is a need, therefore, for sensorless techniques with better performance characteristics.

The aim of this project was to develop a low cost sensorless technique for BLDC motors whose performance is equal to or better than that offered by systems relying on low resolution physical sensors such as those based on Hall sensors. Specific objectives were:

- to carry out preliminary evaluation of candidate sensorless techniques with the potential to satisfy the aim of the project and select the one which is judged to be most promising for detailed analysis;
- to develop analytical tools that would allow detailed analysis of the selected technique;
- practical realisation of the selected technique; and
- to carry out laboratory tests for the practical evaluation of performance of the selected technique.

1.4 Outline of the Dissertation

Chapter 2 is a review of publications that are relevant to this work. As a result of that review it was decided that a saliency based method will be adopted for this project. The presence of saliency (Stölting et al., 2002) results in variation in the response of machine currents and voltages as a function of position. The basic idea is to deduce rotor position information from one or more of those responses. Chapter 3 is devoted to the question of how to induce those responses and which one(s) to use to help determine rotor position. The investigations carried out as part of Chapter 3 led to what is believed to be a novel sensorless technique. This technique which has been termed “the equal inductance method” was selected for detailed analysis and practical implementation.

Detailed analysis of the “equal inductance method” is carried out in Chapter 4. Important objectives of the analysis are to assist with practical implementation and to assess sensitivity and robustness of the method.

Practical implementation of the “equal inductance method” is described in Chapter 5. This includes description of hardware and explanation of key software features. The chapter ends with a discussion of performance tests carried out on a prototype system.

Chapter 6 concludes the dissertation. It includes a summary of project achievements and suggestions for further work.

Chapter 2

Literature review

2.1 Introduction

Sensorless control of permanent magnet machines has been a research topic for more than two decades and this has resulted in a large number of publications dedicated to the subject. As part of this project, some of those have been reviewed. Papers were selected for this review based on their relevance to the aim of developing a low cost method that works down to zero speed. The main objective of the review was to ascertain, through the published work of previous researchers, the range of feasible options that are available for the implementation of a sensorless method for BLDC drives.

The basis of most low and zero speed sensorless controllers is that there exists a difference between direct axis and quadrature axis inductances (Wang & Lorenz, 2000; Ovrebo, 2004; Schmidt et al., 1997; Chiricozzi et al., 1998; Robeischl et al., 2004; Petrovic et al., 2003) or between direct axis and quadrature axis resistances (Leksell et al., 1998). This difference is what was termed ‘saliency’ in Chapter 1. Depending on their construction, there are several sources of saliency in permanent magnet machines. The main sources are: saturation based saliency (yoke, teeth) and rotor inherent saliency.

At higher speeds, the back EMF waveform contains enough information for a satisfactory estimation of the position. Many systems using saliency based methods (example: Robeischl et al., 2004) switch to back EMF based methods at higher speeds. It is therefore beneficial to have a good understanding of the back EMF method which is briefly covered in this review.

2.2 Saturation based methods

In a permanent magnet machine where there is no rotor inherent saliency a saturation induced saliency method can be adopted. In many cases saturation related methods are used to determine initial position. Schmidt et al. (1997) present a technique that allows estimation of the rotor angular position using saturation of the stator iron. Their method works down to standstill and provides absolute rotor position within a pole pair (360 electrical degrees). In Figure 2.1a and 2.1c, phase A winding is aligned with the rotor direct axis. In both cases the flux linking the coil is saturating the stator iron. This is not the case in Figure 2.1b, where phase A winding is aligned

with the rotor quadrature axis and therefore no iron saturation occurs. Since saturated iron reduces the coil inductance, the lowest inductance values of phase A occurs at the direct axis alignment position (Figure 2.1a and 2.1c).

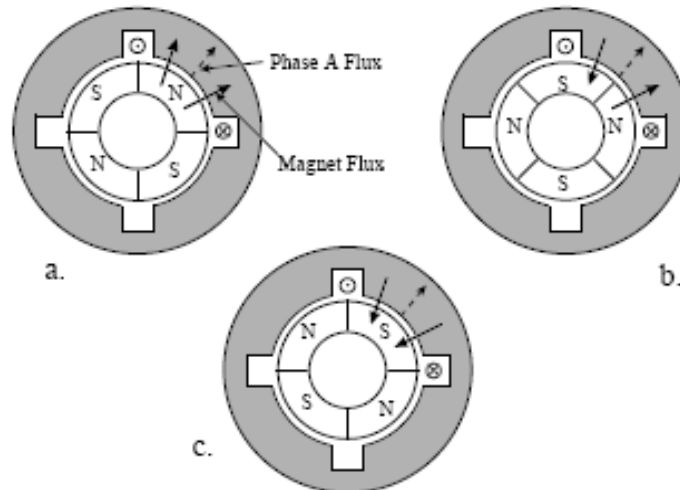


Figure 2.1 : Rotor flux affecting flux produced by phase winding (Source: Schmidt et al., 1997)

When a north pole is magnetically aligned with phase A, the current in the winding causes an increase in flux linked by the winding (Figure 2.1a). This increases stator saturation and slightly decreases the inductance which was present with no stator current. When a south pole is aligned with the coil, the current in the coil causes a decrease in the flux linked by the winding (Figure 2.1c). This decreases stator saturation, and slightly increases the inductance that was present with no stator current. Since the inductance of the winding is different for different rotor pole alignment (Figure 2.2), one can use its value to distinguish the polarity of the rotor pole that is aligned with the winding. Absolute rotor position (within a pole pair) can therefore be deduced

from knowledge of winding inductance which is itself calculated from measured rates of rise of phase current resulting from the application of a known phase voltage.

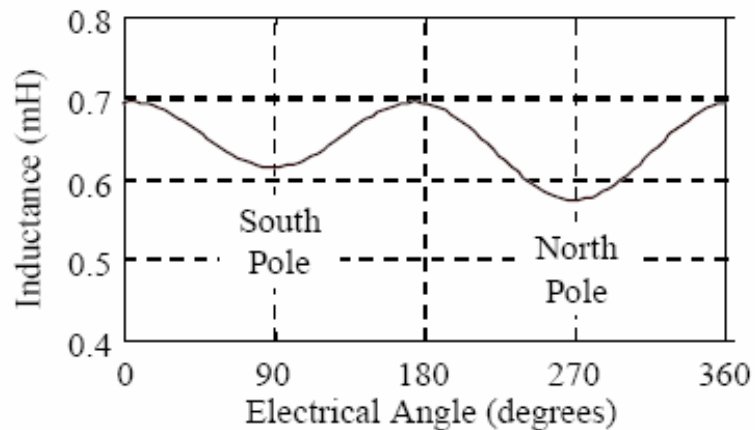


Figure 2.2 : Stator inductance as a function of rotor position (Source: Schmidt et al., 1997)

Chiricozzi et al. (1998) also show how to determine initial position using saturation. The basic principle is similar to the one presented by Schmidt et al. (1997). In the magnetic circuit (Figure 2.1) two effects are superimposed, the permanent magnet flux and the flux due to phase A current. Depending on the sign of the phase current, the flux due to the phase current is added to or subtracted from the permanent magnet flux. In case of an addition, if the phase current is suitably high, the total flux saturates the magnetic circuit and the resulting inductance is low. In case of a subtraction, saturation is not present and this results in a higher winding inductance. A positive voltage pulse is applied and the positive phase current is measured and then forced to zero. The procedure is repeated with a negative voltage pulse and the negative phase current is measured again (Figure 2.3).

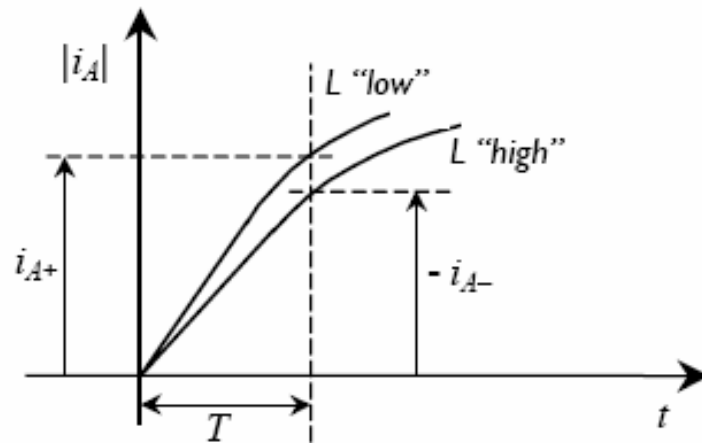


Figure 2.3 : Inductance variation due to saturation (Source: Chiricozzi et al.,1998)

A current difference $(|i_{A+}| - |i_{A-}|)$ can be computed. By applying this procedure to each phase, profiles of current differences over the electrical period are obtained (Figure 2.4).

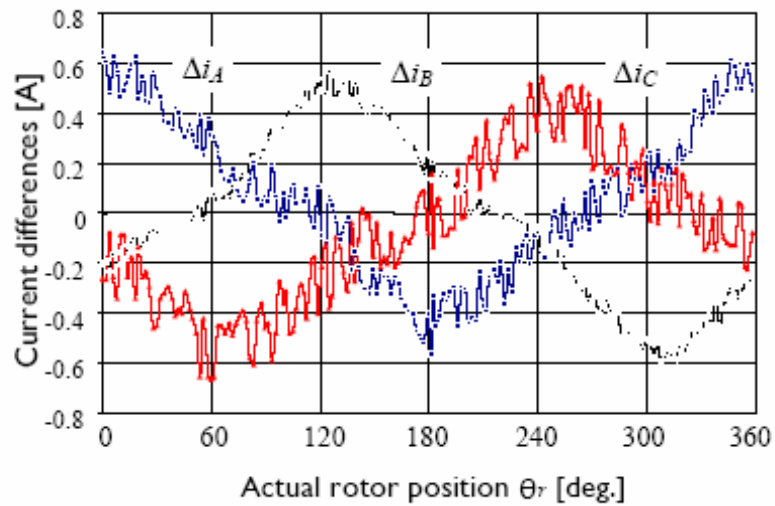


Figure 2.4 : Current differences (Source: Chiricozzi et al.,1998)

If the combination of the signs of the current differences is considered, it is possible to determine the rotor position with a resolution of sixty (electrical) degrees, which is sufficient for the so called six steps commutation purpose.

2.3 Methods based on rotor inherent saliency

Saliency due to the rotor geometry (inherent saliency) is almost unaffected by the stator currents. This makes position sensing algorithms based on such saliency very robust. The magnitude of rotor saliency generally determines the accuracy limits of position sensing.

Sensorless control of permanent magnet machines at low and zero speed requires injection of a test signal to extract information on rotor position. The injection can be explicit as with the INFORM (Indirect Flux Detection by Online Reactance Measurement) method (Robeischl et al., 2004) or indirect (Petrovic et al., 2003).

The basic idea behind the INFORM method (Robeischl et al., 2004) is to measure current responses caused by voltage of both polarities applied in turn to all motor phases and to use those to compute winding inductances. Rotor position can then be deduced from the inductance values. The influence of the back EMF and stator resistances is eliminated by taking pairs of measurements corresponding to different polarities of the applied phase voltage. Phase voltages are applied directly to the permanent magnet machine, by interrupting the PWM pattern for a specific period of time. This causes higher current ripple, additional losses and acoustic noise.

Petrovic et al. (2003) present a method which uses the inherent high-frequency content in motor currents due to the applied PWM stator voltage (instead of auxiliary signal injection). However, they do slightly modify the normal PWM pattern, and their method relies on relatively sophisticated computing algorithms.

Weiss (1998) introduces a method where a predefined sequence of voltages is periodically applied to the machine. The resulting voltage at the inactive motor terminal is measured. Angular position of the rotor is estimated from those measurements.

Ueki (1992) describes a sensorless based method which relies on the effect of saliency on the voltage between the star-point and the negative rail of the DC supply. The method proposed requires a predefined voltage pattern to be applied to all two-phase combinations of the motor. The voltage at the star-point is then measured and rotor position is deduced from those measurements.

2.4 Back EMF based methods

The back EMF is a function of position and is proportional to speed. As mentioned in Chapter 1 detection of position using the back EMF at zero and low speeds is not possible. Nevertheless, there are many applications (example: fans and pumps) that do not require position control or closed-loop operation at low speeds. For these applications, a back EMF based method is quite appropriate. There are many different ways of using the back EMF signal for position sensing

(Sepe & Lang, 1992; Bolognani et al., 1999; Kim & Sul, 1997; Shouse & Taylor, 1998). The majority of these are based on machine terminal voltage sensing and/or star-point voltage sensing.

Widely used, is the so called back EMF “zero crossing” method, where the instants of back EMF zero crossings are used to estimate position (Prokop, 2003). It is important to mention that there is a 30° (electrical) offset between the back EMF zero-crossing and required commutation instant, which must be compensated for to ensure efficient and smooth operation of the motor.

Bosch (1997) describes the development of an economic electrical single spindle drive for textile machines based on detecting the third harmonic components in the back EMF signals. The back EMF signals contain odd harmonics since the air gap flux density has an almost rectangular distribution in space. The third harmonic in all three winding voltages are in phase. Bosch (1997) presents a relatively simple method of third harmonic detection using a star-point connection. The zero-crossings of the third harmonic signal correspond to the successive zero-crossings of the back EMF signals of the three stator phase windings. The main advantage of this method is that only one signal needs to be processed to detect all the required zero-crossing instants.

2.5 Conclusions

The following general conclusions were arrived at after the literature review was completed:

- (a) The adopted method for this project would have to be based on inductive saliency, resistive saliency or a combination of the two.
- (b) The level of sophistication of some of the published methods is probably not needed for this project since accurate rotor position is required only for the purpose of commutation. In other words there is no need for high resolution rotor position sensing.
- (c) As much as possible, the rotor position estimate should be independent of machine parameters such as winding resistances and inductances, inverter transistor voltage drop and DC supply voltage. It should also be independent of the level of the back EMF and the rotor speed.
- (d) Methods based on auxiliary signal injection can be relatively complex and they generate additional torque ripple and power losses that can become excessive.
- (e) Some methods, specially those based on fast evaluation of the rate of rise of current, may require relatively expensive computing hardware.

In relation to the selection of a suitable sensorless control method, the above points led to four fundamental questions that needed answering. These were:

- Would auxiliary signal injection result in excessive complexity and performance deterioration?
- Is the low-cost digital signal processor (DSP) intended to be used for the project powerful enough?
- Is a star-point connection an acceptable compromise?
- If transition from the low speed sensorless method to the back EMF method is necessary, how easy and how smooth is that transition?

Preliminary practical investigations using a selected test motor were carried out to help answer those questions. These investigations and their outcomes are presented in the next chapter.

Chapter 3

Preliminary investigations

3.1 Purpose of Investigations

To help with the task of selecting a sensorless technique with good potential to achieve the aim of this project, it was decided to carry out some preliminary practical investigations. The intention was to find the clues to an economic way of inducing a machine current or voltage response that could be used to detect rotor position. Another objective was to identify and avoid techniques that have undesirable side effects on the machine's performance, for example an excessive increase in torque ripple.

3.2 The test machine

The test machine, which was used for the preliminary investigations was the CM120, supplied by Eltronic Ltd, Switzerland. It is a radial flux toroidally wound machine with eight NdFeB permanent magnets. Magnetic and mechanical properties of the magnets are given in Tables 3.1 and 3.2 respectively. The motor nameplate ratings are given in Table 3.3. The CM120 features quasi surface mounted magnets on the rotor (Figure 3.1).

Table 3.1 : Magnetic properties of the CM120 motor magnets (Source: Bomatec AG)

Grade	Max. Energy Product	Remanence	Coercive Force		Working Temp.
	(BH)max	Br	Hc	Hci	Tw
	kJ/m ³	MT	kA/m	kA/m	°C
N40SH	309-333	1270	>944	>1600	150

Table 3.2 : Physical and mechanical properties of the CM120 motor magnets (Source: Bomatec Ltd)

Density	g/cm ³	7.5
Young's Modulus	GPa	160
Compressive Strength	MPa	1100
Thermal Conductivity	W/(m*K)	9
Electrical Resistivity	uOhm*m	1.5
Specific Heat	J/(kg*K)	420

Table 3.3 : Test Motor Nameplate Data

Rated Voltage (V)	24
Rated Current (A)	2
Rated Speed (rpm)	2400
Number of Poles	8

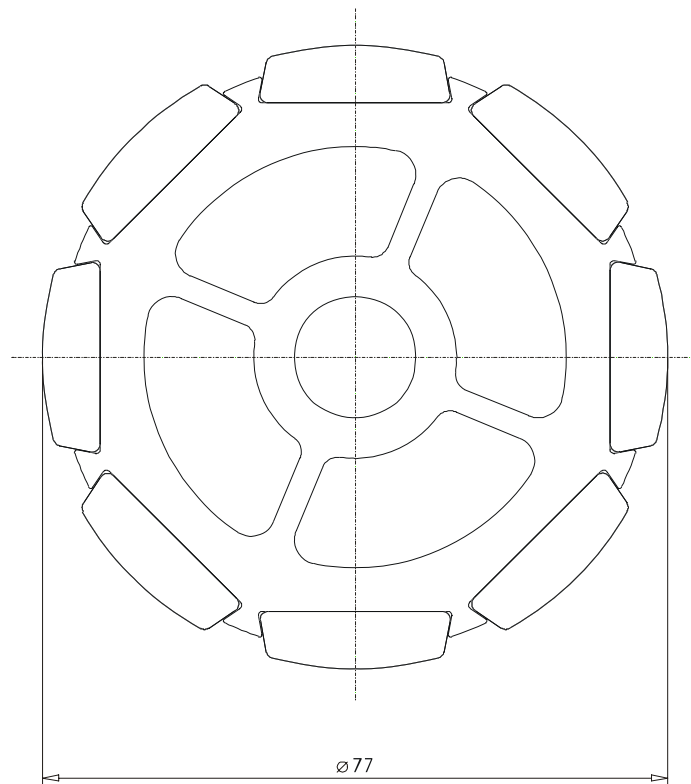


Figure 3.1 : Rotor of the CM120 machine (Source: Eltronic Ltd)

As pointed out in Chapter 2, it was decided to adopt a saliency based method for the project. The CM120 was chosen as the test motor because its construction suggests the presence of saliency.

3.3 Inverter Bridge Operation

In Chapter 1 a typical bridge inverter configuration was introduced. The switching strategy that is normally adopted for the bridge is either the bipolar control method or the unipolar control method (Chalupa 2001). In an attempt to identify opportunities to develop suitable position sensing techniques, it was decided to revisit the basic principles behind the unipolar and bipolar control methods. Only one of the six inverter intervals previously defined in Chapter 1, say interval AB, needs to be considered to adequately explain the relevant principles. Referring to Figure 3.2, during interval AB, transistors T1, T2, T3 and T4 are pulse width modulated whereas transistor T5 and T6 are kept off. In the following analysis, the blanking time that is necessary between the switching of the complementary transistors in an inverter leg has been ignored.

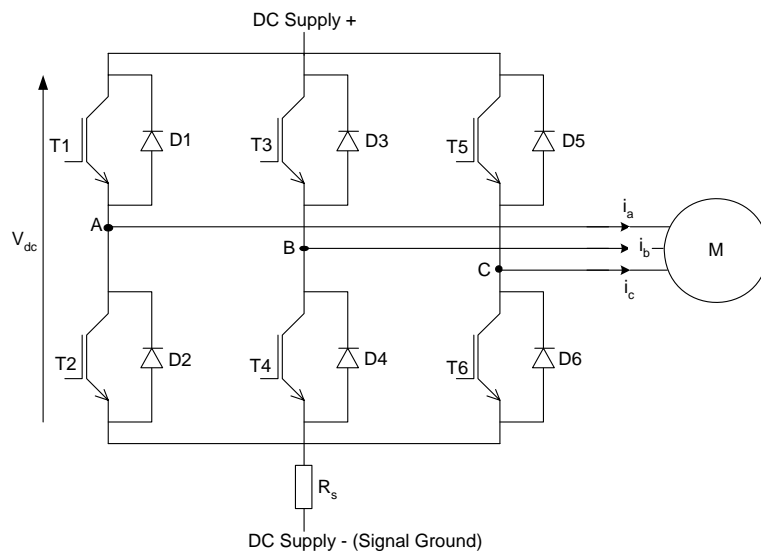


Figure 3.2 : Three Phase Bridge Inverter Connected to BLDC

3.3.1 Unipolar Switching

Refer to figure 3.3. If switching device voltage drops are ignored, during inverter interval AB the motor terminal voltage v_{AB} can assume one of three levels. These are V_{dc} , $-V_{dc}$ and 0. In any one PWM cycle v_{AB} will change alternately between levels V_{dc} and 0 or between levels $-V_{dc}$ and 0 depending on the quadrant that the motor is operating in. The four quadrants are defined as:

- Quadrant 1, forward motoring;
- Quadrant 2, reverse braking;
- Quadrant 3, reverse motoring;
- Quadrant 4, forward braking.

Figure 3.3 is a pictorial representation of the inverter devices that carry the motor current during each subinterval of a PWM cycle. Irrespective of the quadrant that the motor is operating in, there are four subintervals within each PWM cycle. As shown in Figure 3.3 the pair of inverter devices that conduct during each of those subintervals depends on the operating quadrant. For example during forward motoring (Quadrant 1), T1 and T4 carry the motor current during that part of the PWM cycle when power flows from the DC source to the motor. This is shown as configurations 1 and 3 in Figure 3.3. Configurations 2 and 4 (Quadrant 1), correspond to time intervals within the PWM cycle when v_{AB} is equal to zero. In other words during those time intervals the motor will be freewheeling. When freewheeling takes place , the current through the current sensing resistor R_s (Figure 3.2) is equal to zero. This presents a time window, within

each PWM cycle, during which the sensor may be used to monitor short current pulses that can be injected specially for the purpose of position detection. The suitability of such a position detection method is investigated in section 3.4.

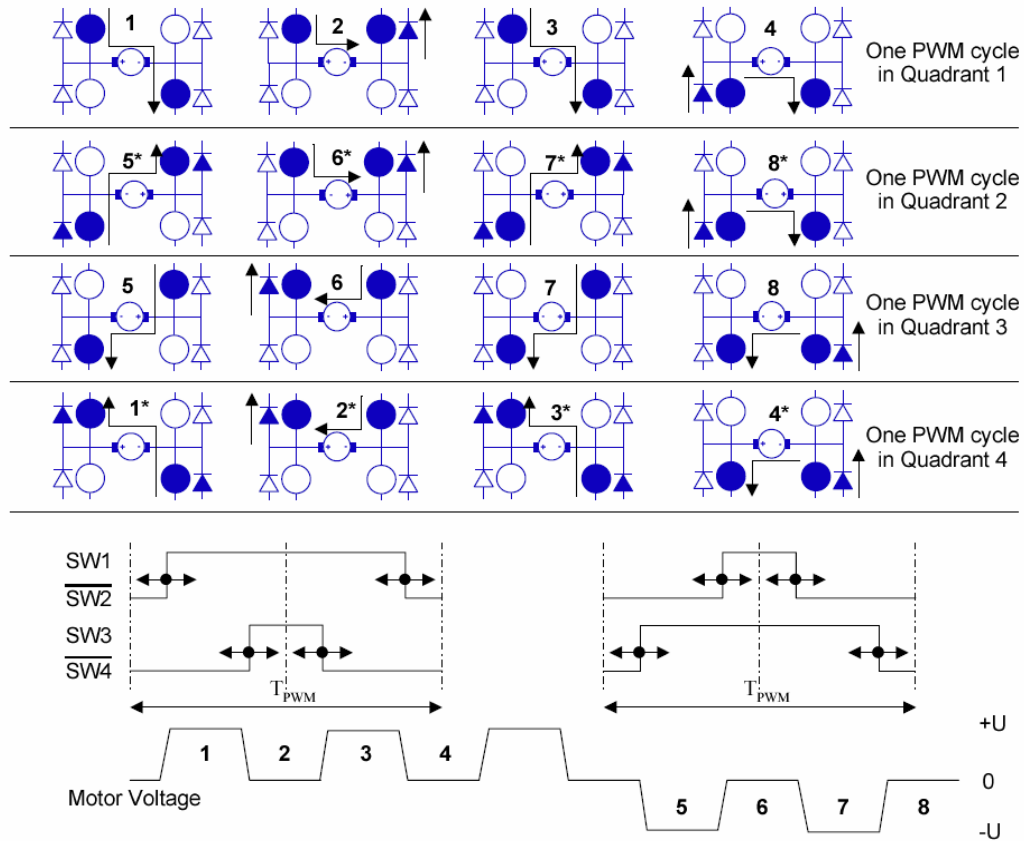


Figure 3.3 : Unipolar Switching strategy (Chalupa, 2001)

3.3.2 Bipolar Switching

Refer to Figure 3.4. If switching device voltage drops are ignored, during inverter interval AB, the motor terminal voltage v_{AB} can assume one of two levels which are $-V_{dc}$ and V_{dc} . Any PWM

cycle v_{AB} can be divided into two subintervals. During one of those v_{AB} is equal to V_{dc} and during the other one v_{AB} is equal to $-V_{dc}$. As shown in Figure 3.4, the pair of devices that carry the motor current during each subinterval depends on the quadrant in which the motor is operating. Unlike the unipolar case, no freewheeling interval exists. This means that generally load current continuously flows through the current sensing resistor making it difficult to use it to monitor any current pulses injected for the purpose of rotor position estimation. However, it was suspected that if the motor is star connected, the pulse width modulated waveform applied across the motor terminals causes saliency related changes in the star point voltage. Test results confirming this are presented in Section 3.5.

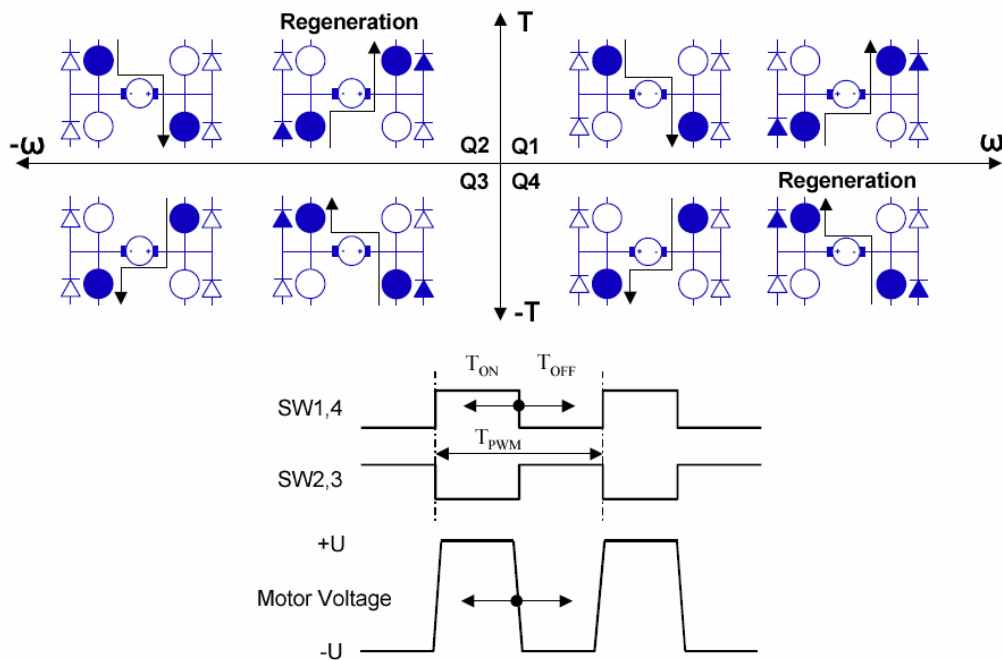


Figure 3.4 : Bipolar Switching Strategy (Chalupa, 2001)

3.4 Pulse Injection

A simple experiment was performed to help assess the practicality of using current pulse injection to detect rotor position. The inverter bridge was connected to the test motor as shown in Figure 3.2. The DC supply voltage was set to 24 V. The transistors T3 and T5 were maintained continuously in the on-state and the motor was held stationary at a desired angular position. For each selected rotor angular position, transistor T2 was switched on for 50 microseconds and then switched off. This closely relates to the practical situation where current injection is carried out during freewheeling intervals. As mentioned in section 3.3.1 the intention was to use current sensor R_s to monitor injected current pulses during freewheeling intervals because it does not carry normal motor current during those intervals. Figure 3.5 shows recorded a-phase current responses for two rotor angular positions. These are, respectively, positions where the magnetic axis of the a-phase aligns with the d-axis and the q-axis.

It is clear that saliency has a small effect on the current responses. It should be pointed out that in practice the current passes through the current sensing resistor R_s only while it is rising, that is during the time when the “pulsed” transistor is on. After that (beyond 50 microseconds in Figure 3.5), the current decays through a freewheeling path and does not pass through R_s . In this case the a-phase current rises through T2 while it is on and then decays through a freewheeling path made up of D1 and one or both of T3 and T5.

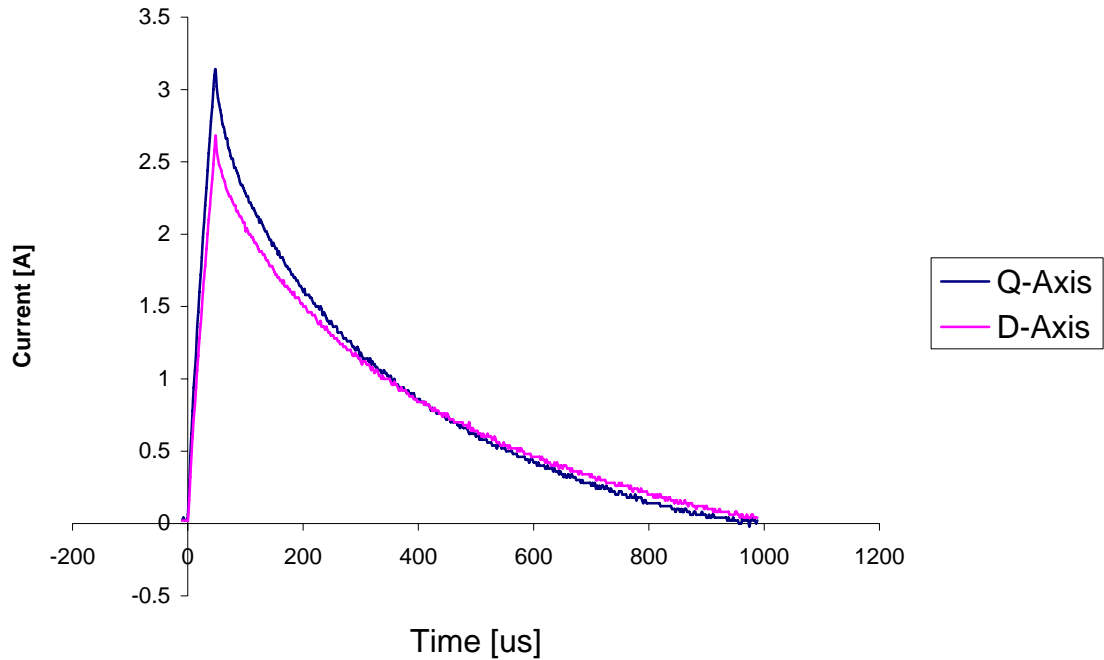


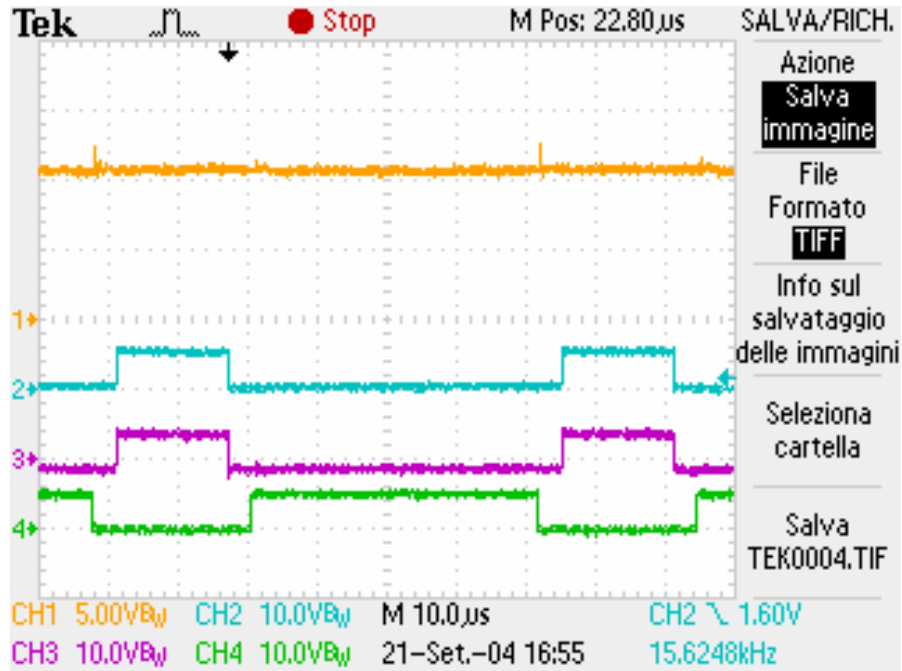
Figure 3.5 : d- and q-axis step response (in alignment with phase A)

It appeared that, provided there is sufficient saliency and accurate high resolution measurements could be done cost-effectively, a rotor position sensing method could be based on the monitoring of injected current pulses using current sensor R_s . However, the decision on whether or not to adopt such a method was postponed until after preliminary tests were performed to allow assessment of an alternate method based on star point voltage monitoring.

3.5 Star-Point Voltage Response

As pointed out before, the voltage applied to an inverter driven BLDC motor may be regarded as a series of alternate positive and negative steps. If the motor had no saliency at all and all phase windings were identical then, in spite of those steps, the star point voltage would remain constant at half the dc supply voltage. Referring to Figure 3.6, it is clear that, for the test motor, at a particular position where the two energized phases have equal inductances the star point voltage is constant at half the dc supply voltage irrespective of inverter states. Note that the star point voltage is the voltage between the motor star point and signal ground (Figure 3.2). If saliency was not present in the motor, then that star point voltage waveform would not change when rotor position changes. But, as mentioned in Section 3.4, the test motor exhibits a small amount of saliency. Variations of the star point voltage waveform resulting from that saliency are shown in Table 3.4. Only the ripple content of the waveform is shown. It is clear that the star-point voltage response carries position information. The star point voltage waveform could be described as a dc voltage equal to half the supply voltage upon which an ac or ripple voltage is superimposed. Because of saliency, the ripple voltage is modulated by the rotation of the rotor. For the test motor, if ringing just after switching is excluded, the peak to peak value of the ac voltage ranges from a maximum of about 1 V down to zero V at the position of equal inductance of the energised phases. It will be shown in the next chapter that the position of equal inductance is also the position of back EMF zero crossing that is used in the back EMF method of determining commutation instants. It appeared that, provided there is enough saliency and

voltage measurements could be done accurately and with enough resolution, a rotor position detection technique based on star-point voltage monitoring could be the right option.



Channel 1 (first from top, orange): star-point voltage(half DC bus voltage)

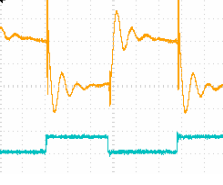
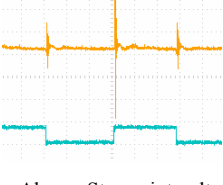
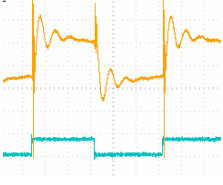
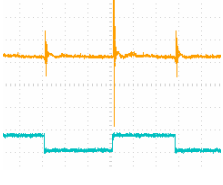
Channel 2 (second from top, blue): switching signal phase A (T2)

Channel 3 (third from top, purple): switching signal phase B (T3)

Channel 4 (fourth from top, green): switching signal phase B (T4)

Figure 3.6 : Star-point voltage waveform

Table 3.4 : Measured Star Point Voltage Waveforms

Rotor position θ (electrical degrees)	Test Waveform Hor.: 10 us/div; Vert.: 500mV/div	Comments
$\Theta=0^\circ$ Direct axis coincides with the magnetic axis of the C-phase.	 <p>Above: Star-point voltage Below: T1 switching signal</p>	Inductances of phase A and phase B are equal
$\Theta=45^\circ$	 <p>Above: Star-point voltage Below: T1 switching signal</p>	Maximum difference between inductances of phase A and phase B
$\Theta=90^\circ$ Quadrature axis coincides with the magnetic axis of the C-phase	 <p>Above: Star-point voltage Below: T1 switching signal</p>	Inductances of phase A and phase B are equal
$\Theta=135^\circ$	 <p>Above: Star-point voltage Below: T1 switching signal</p>	Maximum difference between inductances of phase A and phase B
$\Theta=180^\circ$ Direct axis coincides with the magnetic axis of the C-phase.	 <p>Above: Star-point voltage Below: T1 switching signal</p>	Inductances of phase A and phase B are equal

3.6 The selected Method

The main disadvantage of the current injection method is that to obtain enough resolution the injected current would have to be made sufficiently high. This can only be done at the expense of increasing torque disturbance.

Due to the relatively low values of winding inductance, the current injection method would require current measurements during a short time and at a precise instants after the initiation of the current pulse. Such measurements would have to be done consistently from one PWM cycle to the next. On the other hand monitoring of the star-point voltage is significantly less demanding. The fundamental reason for this is that compared to the rate of rise of the injected current (Figure 3.5), the star point voltage changes very slowly during the interval between inverter switching events (Table 3.4). Indeed it will be shown later that a high precision on the measurement instants within PWM cycles is not a requirement.

After considering all the above arguments the decision was made to develop a technique based on star-point voltage monitoring. The aim of that technique was to identify the rotor position corresponding to equal inductance of the energized phases. For this reason the technique has been named the ‘equal inductance method’. The next chapter is devoted to a detailed theoretical analysis of the method.

Chapter 4

The equal inductance method

4.1 Introduction

This chapter is devoted to the theory behind the equal inductance method. The theory is based on the classical d-q model (Fitzgerald et al., 2003) of electrical machines. The essential features of the model are presented in Section 4.2. In Section 4.3, the model is used to show that there exists a simple relationship between ideal commutation positions and the positions of equal self-inductance. It follows that knowledge of equal self-inductance positions can be used to decide commutation positions. In Section 4.4 it is theoretically demonstrated that the equal self-inductance position can be detected by monitoring the star-point voltage waveform. It is then shown, in Section 4.5, that the estimate of rotor position based on the adopted method is

insensitive to operational parameters, such as PWM duty cycle and speed, or circuit parameters such as armature resistance and power device voltage drops. A technique to detect the rotor initial position is presented in Section 4.6. Section 4.7 is a brief discussion on the transfer to or from the back EMF method of rotor position detection.

4.2 Mathematical Model

Electrical machines that exhibit saliency due to geometry of the field member (usually the rotor) are often analysed using the well established two-axis theory (Fitzgerald et al., 2003). This theory leads to the following expressions for the three-phase winding inductances and mutual inductances:

$$L_{aa} = L_{aa0} + L_{al} + L_{g2} \cos(2\theta) \quad (4.1)$$

$$L_{bb} = L_{aa0} + L_{al} + L_{g2} \cos\left(2\theta + \frac{2\pi}{3}\right) \quad (4.2)$$

$$L_{cc} = L_{aa0} + L_{al} + L_{g2} \cos\left(2\theta - \frac{2\pi}{3}\right) \quad (4.3)$$

$$L_{ab} = L_{ba} = -0.5L_{aa0} + L_{g2} \cos\left(2\theta - \frac{2\pi}{3}\right) \quad (4.4)$$

$$L_{bc} = L_{cb} = -0.5L_{aa0} + L_{g2} \cos(2\theta) \quad (4.5)$$

$$L_{ac} = L_{ca} = -0.5L_{aa0} + L_{g2} \cos\left(2\theta + \frac{2\pi}{3}\right) \quad (4.6)$$

where θ is the electrical angle between the magnetic axis of phase A and the direct axis; L_{ii} is the self inductance of phase i; L_{ij} is the mutual inductance between phase i and phase j; L_{aa0} , L_{al} and

L_{g2} are constants which are independent of θ and, if the effects of saturation are ignored, they are also independent of winding currents.

The question is whether or not equations 4.1 to 4.6 are applicable to BLDCs in general and to the test machine in particular. To answer that question some preliminary test were performed. With the rotor fixed at a number of positions relative to the magnetic axis of phase A, a small sinusoidal current (50mA @ 20kHz) was injected into one phase, while the other two phases were left open circuited. The injected current and the three line to neutral (star-point) voltages were recorded. From the measurements, effective self-inductances and mutual inductances were evaluated. The calculated self-inductances and mutual inductances which are displayed in Figure 4.1 and Figure 4.2 provide justification for using the two-axis theory. In other words the curves in Figure 4.1 and Figure 4.2 are well-represented by equations 4.1 to 4.6.

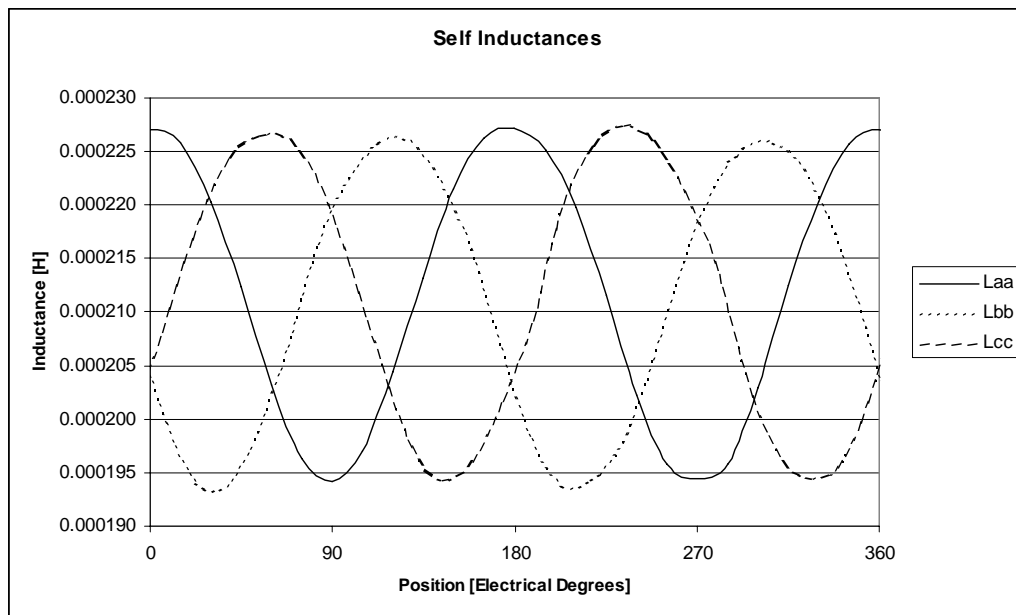


Figure 4.1 : Measured Self-Inductances

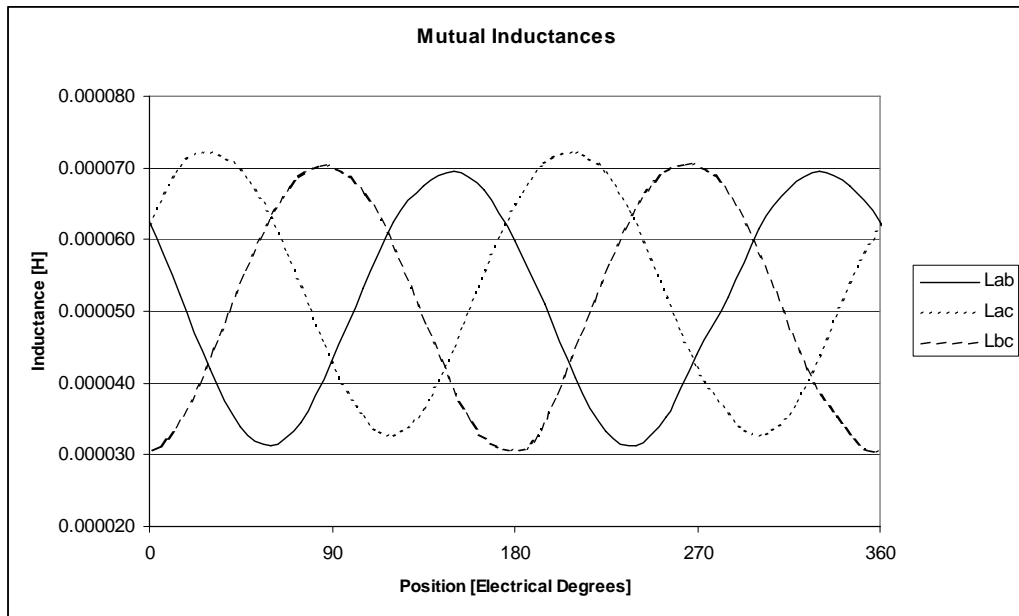


Figure 4.2 : Measured Mutual-Inductances

It should be pointed out that the self-inductances and the mutual inductances are only effective values rather than actual values. The actual value of L_{aa} , for example, can only be obtained from the measurements if all circuits that are magnetically linked to phase A were open-circuited. But that is not possible. Whilst the other two windings were open-circuited, the influence of eddy-currents in the magnets and other parts of the machine could not be eliminated. Therefore the measured winding are lower than the actual values. They may be regarded as effective values that take into consideration the effect of eddy-currents, in a similar manner that the use of sub-transient inductances in synchronous machine analysis is a way of accounting for the effect of damper windings (Kimbark,1955). Because of the effect eddy-currents, the values given in Figure 4.1 and Figure 4.2 will generally depend on frequency. But since we shall be seeking positions of equal inductance, dependence on frequency is not a problem. The important point is

that positions of equal inductance are independent of frequency. The frequency of the test signals (for the determination of the self-inductances and the mutual inductances) was chosen to be 20 kHz, because that is the frequency of the PWM voltage that the test motor is supplied with. However tests performed at other frequencies from 10 kHz to 30 kHz gave similar results.

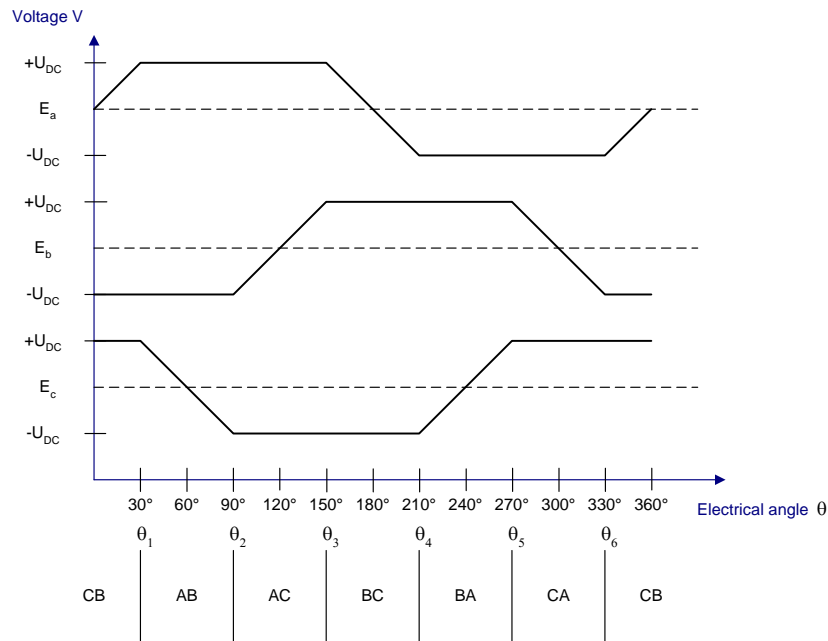


Figure 4.3 : Idealized back EMF waveforms

The mathematical model of the BLDC has to account for the effect of the magnetic field due to the permanent magnets. This is done by the inclusion of rotational back EMFs E_a , E_b and E_c . The following assumptions are made:

- a) The instantaneous values of the back EMFs are proportional to speed

- b) E_a , E_b and E_c are identical to each other except for a phase shift of 120° electrical degrees.
- c) The back EMFs have trapezoidal or quasi sinusoidal profiles as illustrated in Figure 4.3

The above assumptions are supported by open-circuit voltage waveforms obtained with the test machine run as a generator.

For the purpose of explaining and analyzing the ‘equal inductance method’ the following equation will be used to model the BLDC.

$$V = L\dot{I} + (\dot{L}R)I + E \quad (4.7)$$

where:

$$V = [v_a \quad v_b \quad v_c]^T \quad = \text{vector of phase winding voltages}$$

$$I = [i_a \quad i_b \quad i_c]^T \quad = \text{vector of phase winding currents}$$

$$L = \begin{bmatrix} L_{aa} & L_{ab} & L_{ac} \\ L_{ba} & L_{bb} & L_{bc} \\ L_{ca} & L_{cb} & L_{cc} \end{bmatrix} \quad = \text{matrix of phase inductances}$$

$$R = \text{diag}[R_a \quad R_b \quad R_c] \quad = \text{matrix of phase winding resistances}$$

$$E = [E_a \quad E_b \quad E_c] \quad = \text{vector of back EMFs}$$

4.3 Relationship between ideal commutation positions and equal inductance positions

The ideal commutation positions (θ_1 to θ_6) are shown in Figure 4.3. These commutation positions lead to the highest electromagnetic torque per unit ampere as well as the lowest torque ripple. The reason for this is that each phase is energized during the 120 degree intervals centered about the peak value of the phase back EMF.

It follows from the previous paragraph that the zero-crossings of the back EMF of a particular phase occurs 30 electrical degrees before that phase is energized. But the back EMF zero crossing of a phase winding also coincides with alignment of the magnetic axis of that winding with the d-axis of the rotor. Clearly at that position the self-inductance of that phase is a maximum, whereas the inductances of the two other phases will, because of geometric symmetry, be equal to each other. In other words, wherever the rotor d-axis aligns with the magnetic axis of the A-phase winding, E_a is equal to zero and $L_{bb} = L_{cc}$. Similar statements can be made about the B-phase winding and the C-phase winding. Therefore the positions of equal inductance of the energized phases, just like the zero-crossings of the back EMF of the non-energised phase occur 30 electrical degrees before the next commutation position.

Table 4.1 gives positions at which self-inductances are equal. The angles were obtained from equations 4.1 to 4.3. Note that there are twelve such angles. Six of them correspond to the rotor q-axis coinciding with the magnetic axis of each one of the phase windings. The other six

correspond to the rotor d-axis coinciding with the magnetic axis of each one of the phase windings. Only six of these, the ones associated with q-axis alignment will be used to help determine commutation positions. These are given in Table 4.2.

Table 4.1 : Angular positions at which self inductances are equal

Self-inductances	L_{cc}	L_{cc}	L_{aa}	L_{cc}	L_{aa}	L_{bb}	L_{cc}	L_{cc}	L_{aa}	L_{cc}	L_{aa}	L_{bb}
	L_{bb}	L_{aa}	L_{bb}	L_{bb}	L_{cc}	L_{aa}	L_{bb}	L_{aa}	L_{bb}	L_{bb}	L_{cc}	L_{aa}
Angle at which they are equal	0	$\frac{\pi}{6}$	$\frac{\pi}{3}$	$\frac{\pi}{2}$	$\frac{2\pi}{3}$	$\frac{5\pi}{6}$	π	$\frac{7\pi}{6}$	$\frac{4\pi}{3}$	$\frac{3\pi}{2}$	$\frac{5\pi}{3}$	$\frac{11\pi}{6}$

Table 4.2 : Comparison between commutation positions and positions at which self-inductances are equal

Interval	Active Phase	Position where self-inductance of active phases are equal	Next commutation position
CB	c,b	0	$\frac{\pi}{6}$
AB	a,b	$\frac{\pi}{3}$	$\frac{\pi}{2}$
AC	a,c	$\frac{2\pi}{3}$	$\frac{5\pi}{6}$
BC	b,c	π	$\frac{7\pi}{6}$
BA	b,a	$\frac{4\pi}{3}$	$\frac{3\pi}{2}$
CA	c,a	$\frac{5\pi}{3}$	$\frac{11\pi}{6}$

The results given in Table 4.2 form the basis of the proposed commutation algorithm (Figure 4.5). It is assumed that there is negligible change in speed between commutation instants.

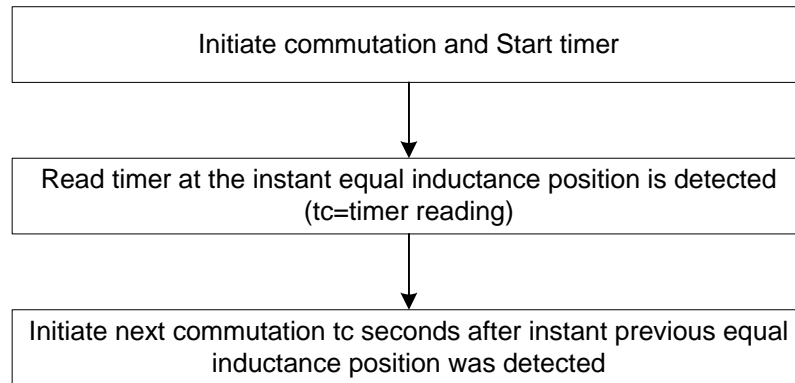


Figure 4.5 : Commutation algorithm

4.4 Detecting Equal Self-Inductance Positions

It is shown, in this section, that equal self-inductance positions of the energized phases can be detected in real time by monitoring the star-point voltage.

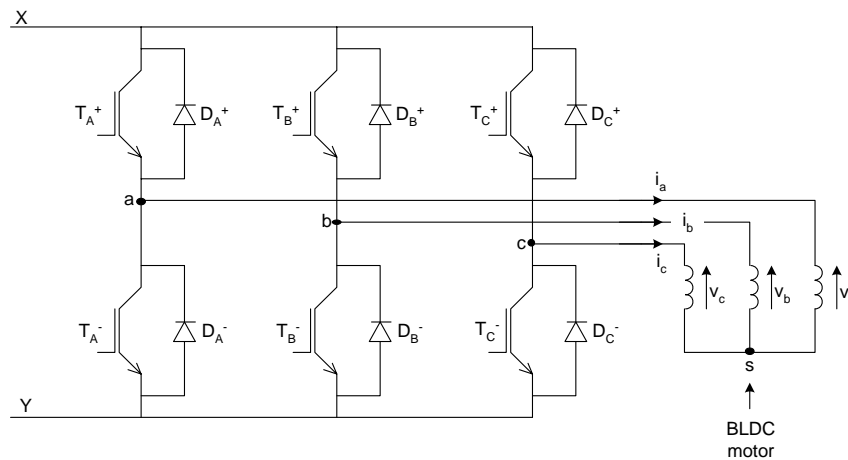


Figure 4.6 : Inverter Bridge Supplying a Brushless DC Motor

As mentioned before there are six commutation intervals. During each interval the aim is to have only two phases active. Transition from one interval to the next involves turning off of one phase and turning on of the next one. This transition is complete only after the current in the outgoing phase has decayed to zero. Decay of the current occurs through a diode (Figure 4.6) and takes finite time. For example the transition from interval AB to interval CB involves decaying current through the diode D_A^- . Therefore each interval involves two sub-intervals, one during which all three-phase currents are present and one during which the non-active phase current is equal to zero. In total there are twelve sub-intervals and twelve corresponding inverter states all of which are shown in Figure 4.7.

The inverter states are labeled as according to the polarity of the DC supply terminal to which the motor phases are connected. For example inverter state $c^+a^+b^-$ implies the “c” and “a” phases are connected, through transistors or diodes to the positive DC rail whereas the “b” phase is connected to the negative DC rail.

Note that since bipolar PWM is used, during any one of the intervals, the inverter may be in one of six possible states. For example during interval AB, the inverter may be in state $a^+c^+b^-$, or $a^+c^-b^-$, or $a^-c^+b^+$, or $a^-c^-b^+$, or a^+b^- , or b^+a^- .

The following main assumptions are made:

- a) During each of the six intervals the inverter operates in bipolar mode;
- b) Inductive saliency is present and may be represented by a sinusoidal function with period equal to 180 electrical degrees;

- c) The three motor phases are identical to each other with their magnetic axes 120 degrees from each other;
- d) The power electronic devices making up the inverter are well-matched;
- e) The effects of magnetic saturation are negligible;
- f) Ripple frequency content in the back emf waveforms is negligible; and
- g) The DC voltage supply to the inverter is sufficiently smooth.

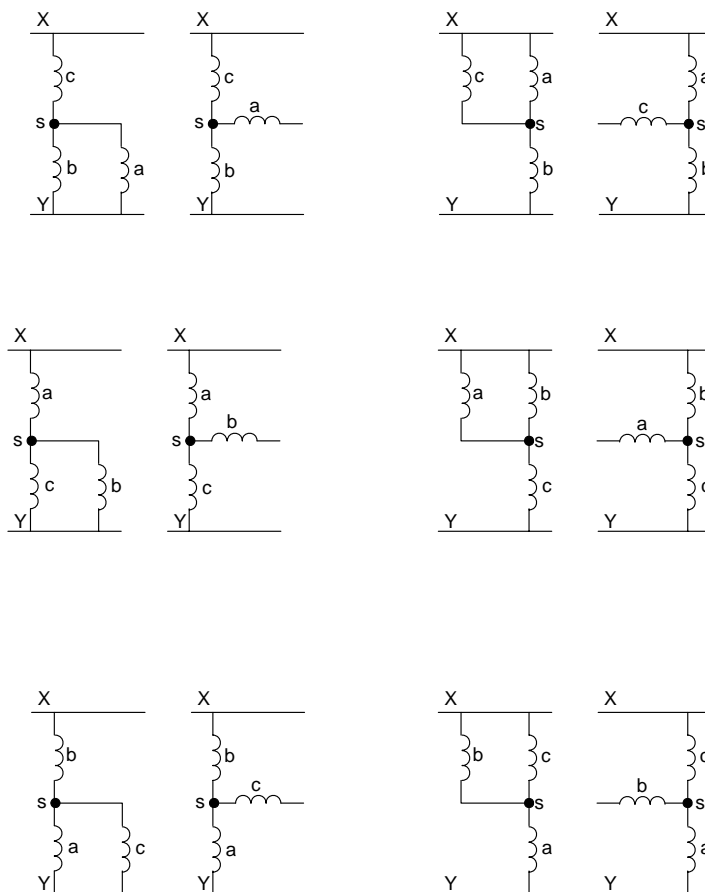


Figure 4.7 : The twelve possible inverter states

The aim is to use inductive saliency to determine the correct commutation instants for the motor. The method is based on the sensing of voltage v_{sy} (Figure 4.6) during the sub-intervals when the non-active phase current has decayed.

Consider interval AB. Assuming current i_c has decayed to zero, the inverter will revert alternately between the states a^+b^- and b^+a^- . These are represented in Figure 4.8.

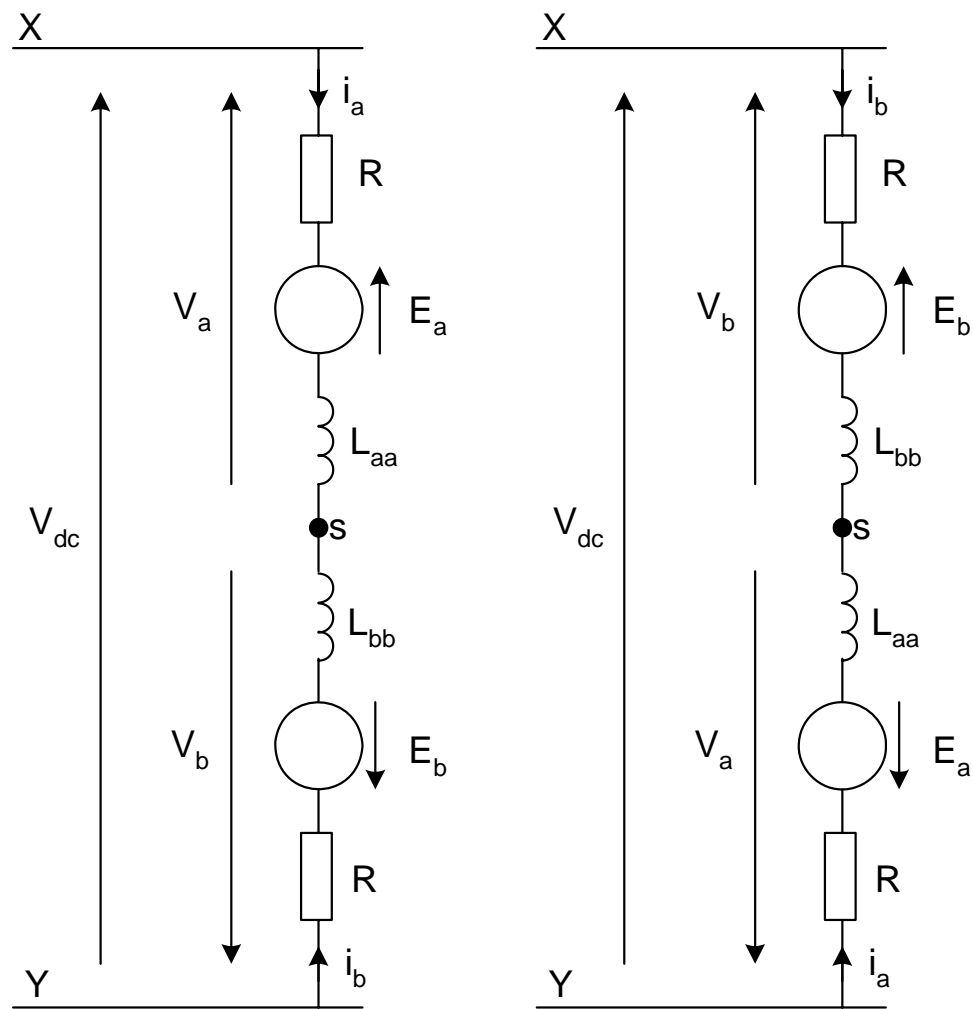


Figure 4.8 : Equivalent circuits for inverter states a^+b^- and b^+a^-

Samples of voltage v_{sy} are continually taken. The sample value corresponding to the current inverter state is compared to the sample value of the previous state. It is shown, in the next paragraphs that those two values are equal to each other at precisely the same rotor position independent of the value of phase current, supply voltage or speed. It is clear then that by simply monitoring voltage signal v_{sy} , rotor position is arrived at with almost zero computational effort. Based on the knowledge of rotor position, commutation instants can be determined.

Consider operation during interval AB. The corresponding equivalent circuits are given in Figure 4.8. Equations 4.8 to 4.11, which can be deduced from equation 4.7 or from figure 4.8, apply irrespective of whether the inverter state is a^+b^- or b^+a^- .

$$v_a = L_{aa} \frac{di_a}{dt} + L_{ab} \frac{di_b}{dt} + i_a \frac{dL_{aa}}{dt} + i_b \frac{dL_{ab}}{dt} + i_a R + E_a \quad (4.8)$$

$$v_b = L_{ab} \frac{di_a}{dt} + L_{bb} \frac{di_b}{dt} + i_a \frac{dL_{ab}}{dt} + i_b \frac{dL_{bb}}{dt} + i_b R + E_b \quad (4.9)$$

Since $i_a = -i_b$,

$$v_a = (L_{aa} - L_{ab}) \frac{di_a}{dt} + i_a \frac{d(L_{aa} - L_{ab})}{dt} + i_a R + E_a \quad (4.10)$$

$$v_b = (L_{ab} - L_{bb}) \frac{di_a}{dt} + i_a \frac{d(L_{ab} - L_{bb})}{dt} - i_a R + E_b \quad (4.11)$$

During inverter state a^+b^- we have:

$$v_{sy^+} = -v_b + V_{t^+} \quad (4.12)$$

$$V_{dc} = v_a - v_b + 2V_{t^+} \quad (4.13)$$

where V_{t^+} is the inverter transistor on-state voltage drop.

From equations 4.10, 4.11 and 4.13 we have:

$$V_{dc} = (L_{aa} + L_{bb} - 2L_{ab}) \frac{di_a}{dt} + i_a \frac{d(L_{aa} + L_{bb} - 2L_{ab})}{dt} + 2i_a R + (E_a - E_b) + 2V_{t^+} \quad (4.14)$$

From Table 4.2 and Figure 4.3, it is found that at the positions where L_{aa} and L_{bb} are equal E_a and E_b are equal and opposite to each other. Therefore at the position of equal inductance we have:

$$V_{dc} = 2(L_{bb} - L_{ab}) \frac{di_a}{dt} + 2i_a \frac{d(L_{bb} - L_{ab})}{dt} + 2i_a R - 2E_b + 2V_{t^+} \quad (4.15)$$

From equations 4.11, 4.12 and 4.15 we deduce that at the position where the self-inductances are equal we have:

$$v_{sy^+} = \frac{V_{dc}}{2} \quad (4.16)$$

During inverter state b^+a^- we have:

$$v_{sy^-} = -v_a - V_{t^-} \quad (4.17)$$

$$V_{dc} = v_b - v_a - 2V_{t^-} \quad (4.18)$$

where V_{t^-} is the inverter diode on-state voltage drop.

From equations 4.10, 4.11 and 4.18 we have:

$$V_{dc} = -(L_{aa} + L_{bb} - 2L_{ab}) \frac{di_a}{dt} - i_a \frac{d(L_{aa} + L_{bb} - 2L_{ab})}{dt} - 2i_a R - (E_a - E_b) - 2V_{t^-} \quad (4.19)$$

At the position of equal inductance we have:

$$V_{dc} = -2(L_{aa} - L_{ab}) \frac{di_a}{dt} - 2i_a \frac{d(L_{aa} - L_{ab})}{dt} - 2i_a R - 2E_b - 2V_{t^-} \quad (4.20)$$

From equations 4.10, 4.17 and 4.20 we deduce that at the position where the self-inductances are equal we have:

$$v_{sy^-} = \frac{V_{dc}}{2} \quad (4.21)$$

Equations 4.17 and 4.21 imply that when the rotor reaches the position where L_{aa} is equal to L_{bb} , consecutive sample values of v_{sy} will be equal to each other. Equality of consecutive values of v_{sy} at a particular angular position indicates that the self-inductances of the active phases are equal at that position. This in turn indicates that commutation should take place exactly after an additional 30 electrical degrees of rotation.

In the next section it is shown that away from the position of equal self-inductance, the values of v_{sy} alternate above and below $V_{dc}/2$ as the inverter alternates between states a^+b^- and b^+a^- . The further away the rotor position is from the point of equal self-inductance, the higher the deviations are between consecutive values of v_{sy} . The maximum deviations between consecutive values of v_{sy} is a measure of the sensitivity of the proposed method of rotor position sensing. The principal factors affecting this sensitivity are investigated in the next section.

4.5 Sensitivity of the proposed position sensing method

With the inverter in state a^+b^- , equation 4.14 is applicable and it may be written as:

$$\frac{V_{dc}}{2} = \left(\frac{L_{aa} + L_{bb}}{2} - L_{ab} \right) \frac{di_a}{dt} + i_a \frac{d \left(\frac{L_{aa} + L_{bb}}{2} - L_{ab} \right)}{dt} + i_a R + \left(\frac{E_a - E_b}{2} \right) + V_{r^+} \quad (4.22)$$

From equations 4.11, 4.12 and 4.22, we get:

$$v_{sy^+} = \frac{V_{dc}}{2} + \left(\frac{L_{bb} - L_{aa}}{2} \right) \frac{di_a}{dt} + i_a \frac{d\left(\frac{L_{bb} - L_{aa}}{2} \right)}{dt} - \left(\frac{E_b + E_a}{2} \right) \quad (4.23)$$

With the inverter in state b⁺a⁻, equation 4.19 is applicable and it may be written as:

$$\frac{V_{dc}}{2} = - \left(\frac{L_{aa} + L_{bb}}{2} - L_{ab} \right) \frac{di_a}{dt} - i_a \frac{d\left(\frac{L_{aa} + L_{bb}}{2} - L_{ab} \right)}{dt} - i_a R - \left(\frac{E_a - E_b}{2} \right) - V_{r^-} \quad (4.24)$$

From equations 4.10, 4.17 and 4.24, we get:

$$v_{sy^-} = \frac{V_{dc}}{2} - \left(\frac{L_{aa} - L_{bb}}{2} \right) \frac{di_a}{dt} - i_a \frac{d\left(\frac{L_{aa} - L_{bb}}{2} \right)}{dt} - \left(\frac{E_b + E_a}{2} \right) \quad (4.25)$$

From Equations 4.23 and 4.24 we have:

$$v_{sy^+} = \frac{V_{dc}}{2} + \left(\frac{L_{bb} - L_{aa}}{2} \right) \frac{di_a}{dt} + i_a \frac{d\left(\frac{L_{bb} - L_{aa}}{2} \right)}{dt} - \left(\frac{E_b + E_a}{2} \right) \quad (4.26)$$

$$v_{sy^-} = \frac{V_{dc}}{2} + \left(\frac{L_{bb} - L_{aa}}{2} \right) \frac{di_a}{dt} + i_a \frac{d\left(\frac{L_{bb} - L_{aa}}{2} \right)}{dt} - \left(\frac{E_b + E_a}{2} \right) \quad (4.27)$$

$$\left(\frac{L_{bb} - L_{aa}}{2} \right) = \frac{\sqrt{3}}{2} L_{g2} \cos\left(2\theta + \frac{5\pi}{6} \right) \quad (4.28)$$

When the inverter is in state a^+b^- , equation 4.22 is applicable and

$$\frac{di_a}{dt} = \frac{\left(\frac{V_{dc}}{2} - i_a \frac{d\left(\frac{L_{aa} + L_{bb} - L_{ab}}{2}\right)}{dt} - \frac{E_a - E_b}{2} - V_{r^+} - i_a R \right)}{\left(\frac{L_{aa} + L_{bb} - L_{ab}}{2}\right)} \quad (4.29)$$

When the inverter is in state b^+a^- , equation 4.24 is applicable and

$$\frac{di_a}{dt} = \frac{\left(-\frac{V_{dc}}{2} + i_a \frac{d\left(\frac{L_{aa} + L_{bb} - L_{ab}}{2}\right)}{dt} + \frac{E_a - E_b}{2} + V_{r^-} + i_a R \right)}{\left(\frac{L_{aa} + L_{bb} - L_{ab}}{2}\right)} \quad (4.30)$$

The denominator in equation 4.29 and equation 4.30 varies with position between L_d and L_q where:

$$L_d = L_{al} + \frac{3}{2}(L_{aa0} + L_{g2}) \quad (4.31)$$

and

$$L_q = L_{al} + \frac{3}{2}(L_{aa0} - L_{g2}) \quad (4.32)$$

Based on typical saliency that would be expected in practice it can be argued that the difference between L_d and L_q would be no more than about 15 per-cent of their average value. Therefore although the denominator in equations 4.29 and 4.30 varies with position, it could be replaced by:

$$\frac{L_d + L_q}{2}$$

Hence the difference between consecutive measurements of v_{sy} is given by:

$$v_{sy^+} - v_{sy^-} = \frac{V_{dc} \left(\frac{\sqrt{3}}{2} \cdot L_{g2} \cos \left(2\theta + \frac{5\pi}{6} \right) \right)}{\frac{L_d + L_q}{2}} \quad (4.33)$$

Since $(V_{t^+} - V_{t^-})$ is much smaller than V_{dc} , this term has been neglected in deriving equation 4.33. Based on equation 4.33 we can conclude that, provided inverter pulse widths are sufficiently short, the rotor position where consecutive values of v_{sy} become equal is independent of all operational or circuit parameters.

Sensitivity or precision of the proposed position detection technique depends only on the ratio

$$\frac{V_{dc} (L_d - L_q)}{L_d + L_q}$$

4.6 Detection of rotor initial position

It has been the aim of this project to develop a sensorless technique with performance characteristics equal to or better than that offered by systems relying on low resolution devices such as Hall sensors (Section 1.3). The theoretical analysis in the previous sections suggests that the equal inductance method has potential to be as good as the Hall sensor based method during normal running of the motor. In this Section it is shown that it is possible to use saliency based information to achieve starting performance characteristics very close to those realised when the Hall sensors are used.

The proposed rotor initial position detection method relies on the fact that measurements of the star-point voltage can be used to compare the magnitudes of phase winding inductances.

Combination of Equations 4.28 and 4.33 gives:

$$L_{bb} - L_{aa} = \frac{\left(v_{sy^+} - v_{sy^-} \right) \left(\frac{L_d + L_q}{2} \right)}{V_{dc}} \quad (4.34)$$

From equation 4.34, it is clear that if v_{sy^+} is greater than v_{sy^-} then L_{bb} is greater than L_{aa} . Note that in the case of equation 4.34 v_{sy^+} corresponds to measurements of the star-point voltage with the inverter in state a^+b^- (see left hand side equivalent circuit of Figure 4.8). Similarly v_{sy^-} in Equation 4.34 corresponds to measurements of the star-point voltage with the inverter in state b^+a^- (see right hand side equivalent circuit of Figure 4.8). Equations similar to 4.34 may be written for the other pairs of self-inductances.

The algorithm for the proposed rotor initial position detection method is based on the flow chart shown in Figure 4.9. Fifty per-cent PWM duty cycle is used at first to prevent rotation. Phase pairs AB, AC and BC are energised in turn. From the six star-point measurements, the ascending order of the three self inductances may be determined. From this the two possibilities for the rotor position range may be deduced (Table 4.3). Inductances L_{\min} and L_{mid} can be identified as shown in Table 4.3. By energising a phase pair defined in Table 4.3, identification of the rotor position range can be based on whether $(L_{\text{mid}}-L_{\min})$ tends to

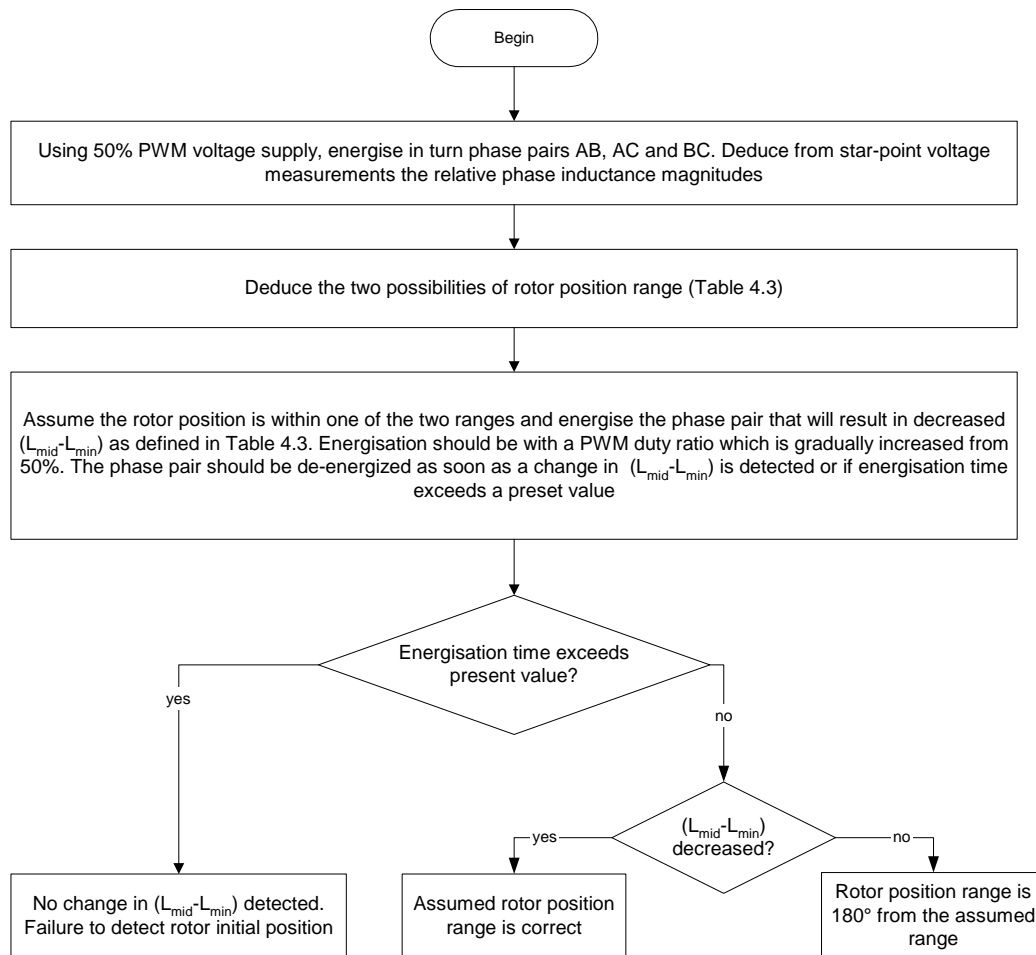


Figure 4.9 : Algorithm for rotor initial position detection

Increase or decrease as the PWM ratio changes from fifty per-cent. For example if the rotor position range is either the first one or the seventh one in Table 4.3, then energisation of phase pair BA allows the actual range to be identified. If energisation of phase pair BA leads to decreasing ($L_{bb}-L_{aa}$) as PWM ratio changes from fifty per-cent then the rotor position range is the first one.

Table 4.3 : Look-up table for detection of initial rotor position

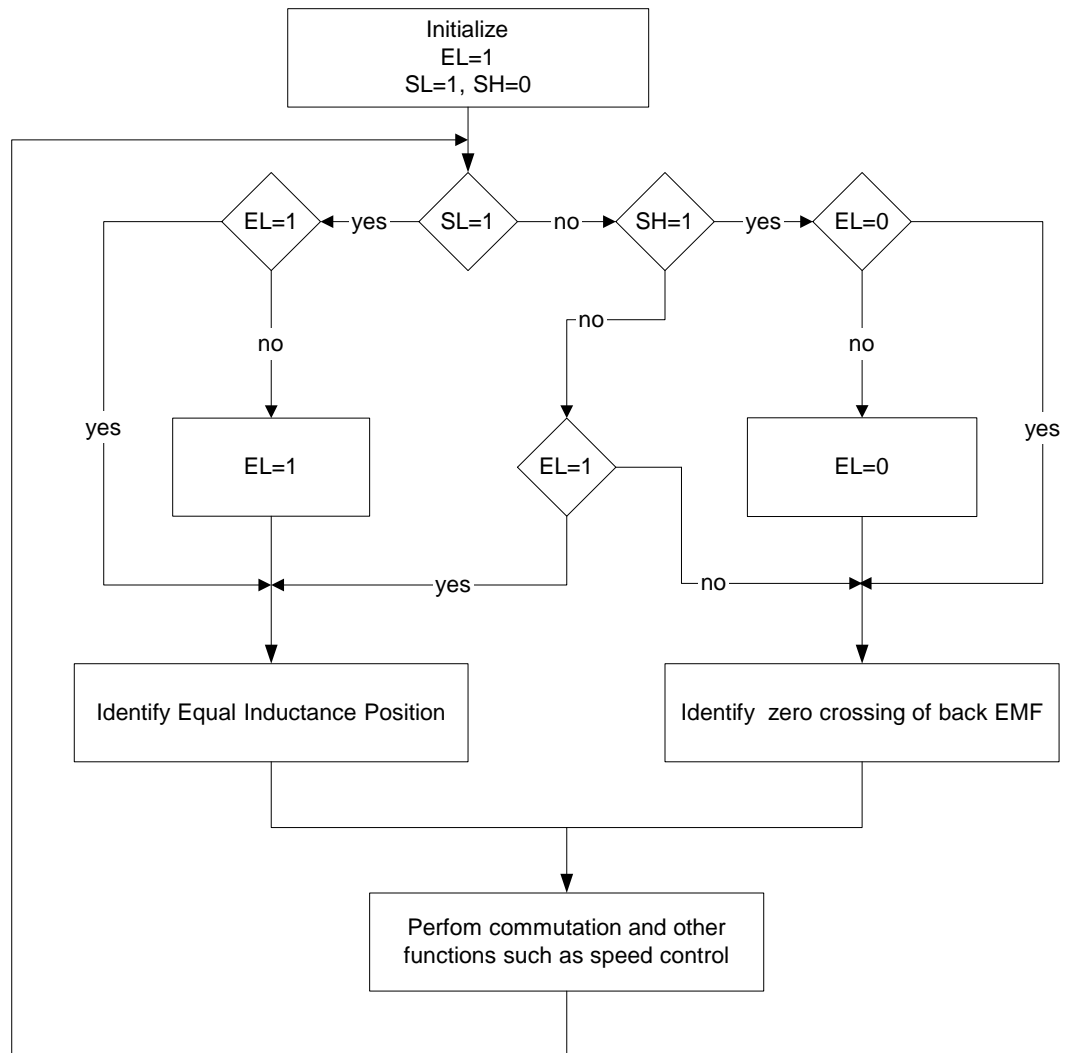
Relative Inductance Magnitude	L_{cc} > L_{bb} > L_{aa}	L_{bb} > L_{cc} > L_{aa}	L_{bb} > L_{aa} > L_{cc}	L_{aa} > L_{bb} > L_{cc}	L_{aa} > L_{cc} > L_{bb}	L_{cc} > L_{aa} > L_{bb}	L_{cc} > L_{bb} > L_{aa}	L_{bb} > L_{cc} > L_{aa}	L_{bb} > L_{aa} > L_{cc}	L_{aa} > L_{bb} > L_{cc}	L_{aa} > L_{cc} > L_{bb}	L_{cc} > L_{aa} > L_{bb}
Rotor Position Range	Θ_2-30 to Θ_2	Θ_2 to Θ_2+30	Θ_3-30 to Θ_3	Θ_3 to Θ_3+30	Θ_4-30 to Θ_4	Θ_4 to Θ_4+30	Θ_5-30 to Θ_5	Θ_5 to Θ_5+30	Θ_6-30 to Θ_6	Θ_6 to Θ_6+30	Θ_1-30 to Θ_1	Θ_1 to Θ_1+30
Lowest Inductance (L_{min})	L_{aa}	L_{aa}	L_{cc}	L_{cc}	L_{bb}	L_{bb}	L_{aa}	L_{aa}	L_{cc}	L_{cc}	L_{bb}	L_{bb}
Middle Inductance (L_{mid})	L_{bb}	L_{cc}	L_{aa}									
Phase pair energisation leading to decreased ($L_{mid}-L_{min}$)	BA	AC	CA	BC	CB	BA	AB	CA	AC	CB	BC	AB
Phase pair energisation leading to increased ($L_{mid}-L_{min}$)	AB	CA	AC	CB	BC	AB	BA	AC	CA	BC	CB	BA

On the other hand if $(L_{bb}-L_{aa})$ increases then the rotor position range is the seventh one. Note that phase pair energisation to determine which one of the pair of rotor position ranges is the right one will, in fifty per-cent of situations, lead to a few degrees of back-rotation.

Once the rotor position range has been identified, the rotor then can be aligned by using the appropriate phase pair and the normal commutation process can follow. For example if the identified rotor position range was the first one in Table 4.3 and the desired direction of rotation was forward (Figure 1.6), then phase pair AB would be used for alignment. Subsequent commutation intervals will be BC, BA, CA and so on.

4.7 Transfer to or from the back EMF method

It may be advantageous in applications where the speed range is wide to transfer to the back EMF method above a certain speed. The fact that the zero crossing of the back EMF of the unenergised phase coincides with the position at which the self-inductances of the energized phases are equal simplifies transfer from the equal inductance method to the back EMF method and vice-versa. A transfer scheme is suggested in Figure 4.10. The transfer scheme include hysteresis (Figure 4.11) to avoid instability near the transition speed. Refer to Figure 4.10. It is assumed that operation starts from standstill. All the three flags (defined in Figure 4.10) are initialized before the start of rotation. At speeds lower than s_{low} (Figure 4.11), the equal inductance method is used. At speeds higher than s_{high}



- SL =low speed flag
- SH =high speed flag
- EL =equal inductance method enable flag

Figure 4.10 : Transfer to or from the back EMF method

the back EMF method is used. Transition from the equal inductance method to the back EMF method occurs at speed s_{high} whereas transition from the back EMF method to the equal inductance method occurs at speed s_{low} .

Note that once the position of equal inductance or the zero crossing of the back EMF has been identified the two methods follow exactly the same process which includes performing of commutation and other functions such as speed control. Instead of using speed measurements to determine the status of flags SL and SH, it is more convenient to use time intervals which, for example, can be measured between instants commutation is initiated or between instants equal inductance (back EMF zero crossing) occur.

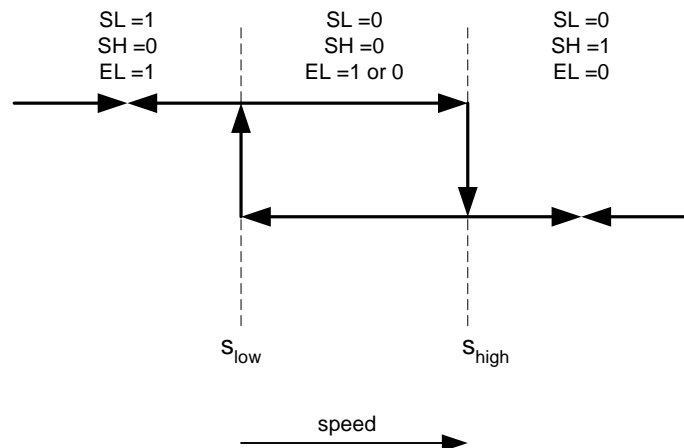


Figure 4.11 : Change of state of EL flag with speed

Chapter 5

Practical implementation

5.1 Introduction

The core feature of any system using the equal inductance method would be commutation control based on detection of instants at which the rotor achieves equal inductance positions.

Example of optional features are:

- start-up, with minimum back rotation, using saliency related measurements (Section 4.6);

- a transfer strategy from low speed operation (equal inductance method) to high speed operation (back EMF method) and vice-versa (Section 4.7); and
- closed-loop speed control.

In this project, only the core feature of the equal inductance method has been implemented.

As expected, the practical realisation of the equal inductance method involves hardware as well as software. An overall system model is given in Figure 5.1. The BLDC motor is the one described in Section 3.2. Relevant details of the hardware interface and the software algorithm are presented in Sections 5.2 and 5.3 respectively. Test results are reported in Section 5.4.

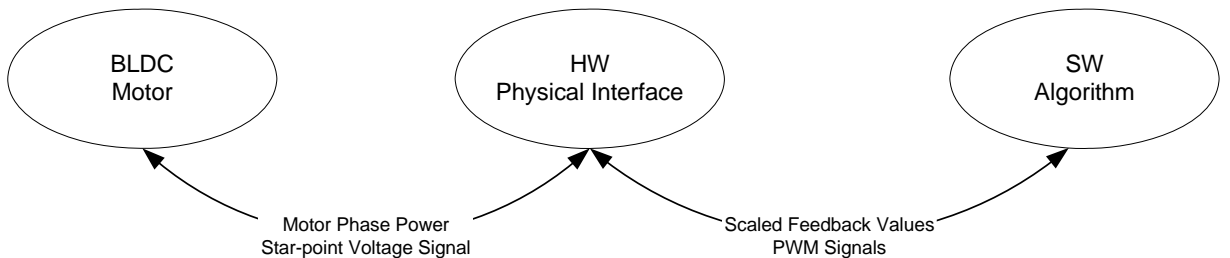


Figure 5.1 : Overall System Model

5.2 Hardware description

5.2.1 Overview

A block diagram of the hardware is given in Figure 5.2. Physically the hardware consists of three connected sections: the BLDC motor, the inverter bridge and the control module.

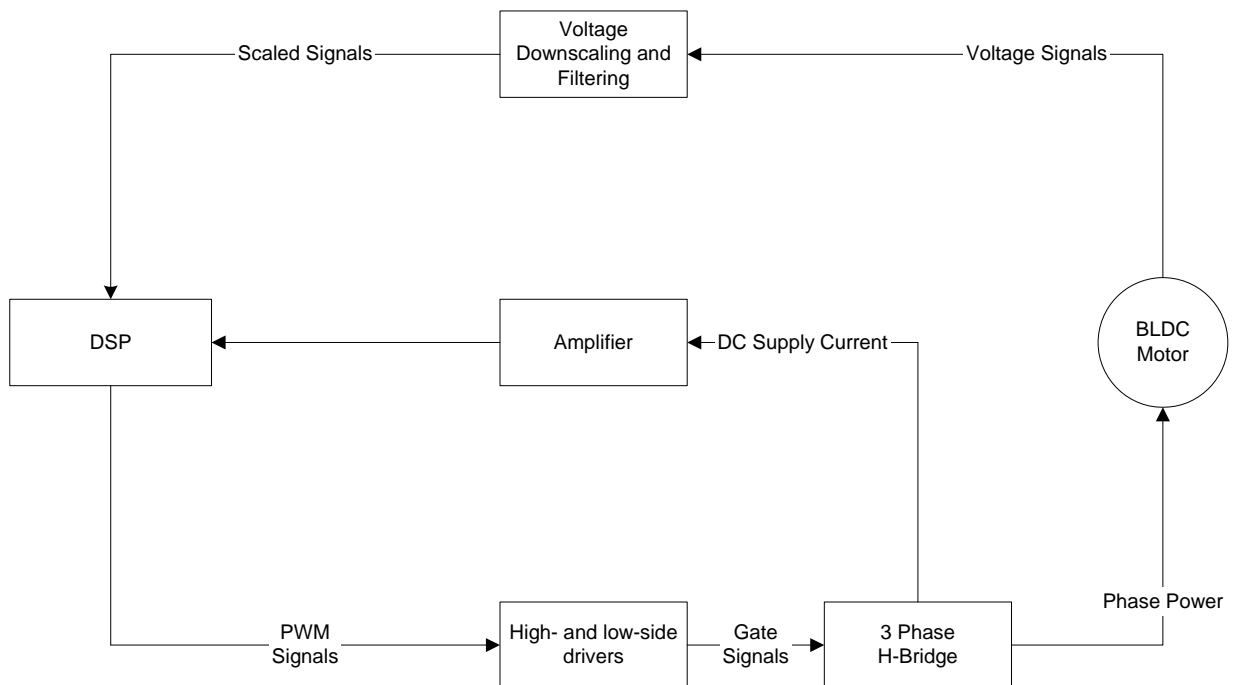


Figure 5.2 : Hardware Block Diagram

5.2.2 The Control Module

Details of the control module are given in Figure 5.3. Metallux Switzerland SA, the firm funding this project intends to use this single control module for all the motor control strategies that they have developed or are developing. These include strategies based on shaft encoders, Hall sensors and the equal inductance method. Therefore some of the circuit blocks shown in the module, for example the ‘feedback signals preprocessing’ block, are not relevant to this project.

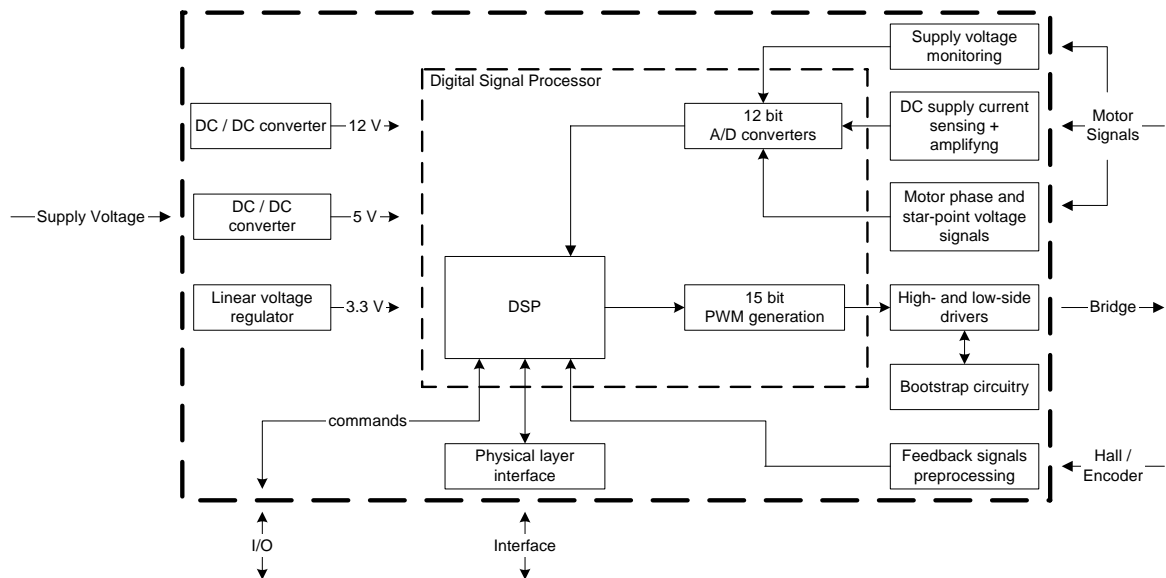


Figure 5.3 : The Control Module

5.2.3 The selected DSC

The heart of the controller is the 56F8013 which is a member of the 56800E family of digital signal controllers (DSCs) (Freescale, 2005). It combines, on a single chip, the processing power of a DSP and the functionality of a microcontroller with a flexible set of peripherals. Because of its low cost, configuration flexibility, and compact program code, the 56F8013 is well-suited for many applications. The 56F8013 includes many peripherals that are especially useful for industrial control, motion control and general purpose inverters. A key application-specific feature of the 56F8013 is the inclusion of one Pulse Width Modulator (PWM) module. This module incorporates three complementary, individually programmable PWM signal output pairs and is also capable of supporting six independent PWM functions to enhance motor control functionality.

5.2.4 The H-bridge

In Figure 5.3 it can be seen that high and low side drivers have been integrated, with the advantage that N-Channel MOSFETs can be used for both, the high and the low side of the bridge. It should be noted that the common connection for the gate drivers is not the general ground, but the source terminals of the low side MOSFETs (Figure 5.4). This prevents the voltage across the shunt resistor (used for current sensing) from interfering with the gate to source voltages. The general ground is the negative terminal of the power supply.

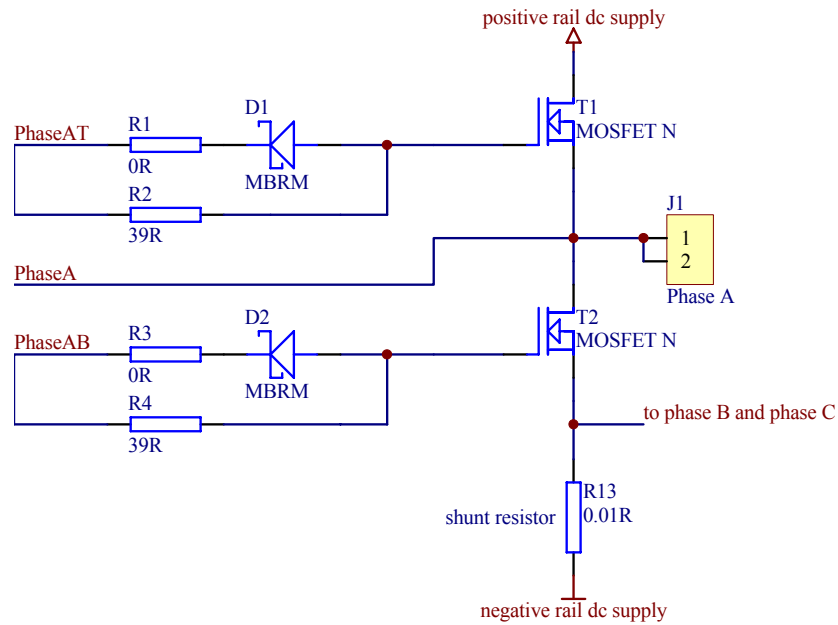


Figure 5.4 : MOSFET and shunt connections

One of the more important design decisions for a motor drive is selection of the gate drive impedance for the output transistors. In Figure 5.6, resistors R1, R2 and diode D1 determine gate drive impedance for the upper half-bridge transistor. A similar network is used on the lower half-bridge. The networks set turn-on gate drive impedance at approximately 39 ohms and turn-off gate current to approximately 500 mA. These values produce transition times of approximately 66 ns. Transition times of this length represent a carefully weighted compromise between power dissipation and noise generation. Generally, transition times longer than 250 ns tend to cause excessive power loss at non-audible PWM rates and transition times under 50 ns create di/dt 's so large that proper operation is difficult to achieve.

5.3 Layout and PCB Manufacturing

The bottom-layer of the control module PCB is shown in Figure 5.5. The PCB, with component mounted, is shown in Figure 5.6. Surface mount components have been used to minimize the size of the module.

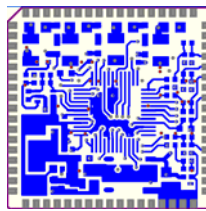


Figure 5.5 : Bottom-layer of the control module

The firm which is funding the project (Metallux Switzerland SA) has the facilities to use alternative technologies such as tick film and flip chip to further reduce the module size.

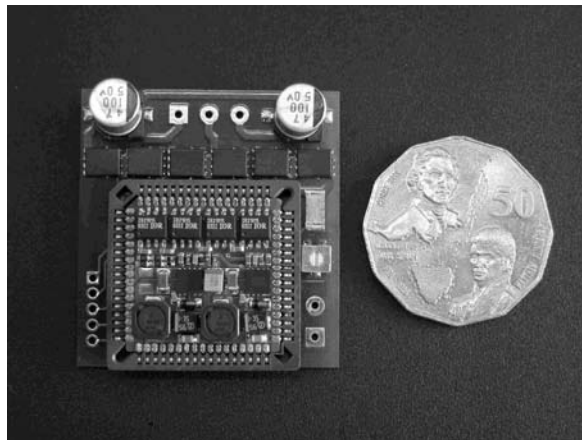


Figure 5.6 : The drive (control module and power semiconductors)

5.4 Software Description

5.4.1 Overview

Figure 5.7 provides an overview of the software in the form of a state diagram.

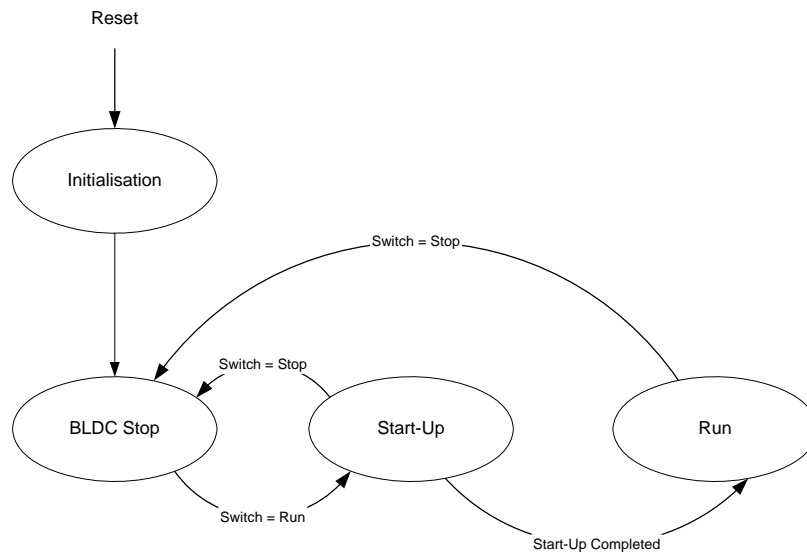


Figure 5.7 : State Transition Diagram

The software has been organised such that once the reset button has been pressed and the DSP initialisation is complete, the system assumes the ‘stop’ state. It remains in the ‘stop’ state as long as the run/stop switch is in the ‘stop’ position. There are two other possible system states, the ‘start-up’ state and the ‘run’ state. When the ‘run/stop’ switch position changes from ‘stop’ to ‘run’, the system leaves the ‘stop’ state and enters the ‘start-up’ state. Details of the ‘start-up’ state are provided in the section 5.4.4. The ‘run’ state is entered after completion of the ‘start-up’

process. The system leaves either the 'run' or the 'start-up' state and enters the 'stop' state anytime the position of the 'run/stop' switch is changed to 'stop'. The commercial version of the software will include a drive 'emergency stop' state. The system will enter that state when a fault such as over-current or over-temperature is detected.

5.4.2 Program structure

The main program (Figure 5.8) is in the form of an endless loop. Various interrupt subroutines (ISRs) are invoked from within the main program. On completion of a particular ISR, program control is returned to the main program.

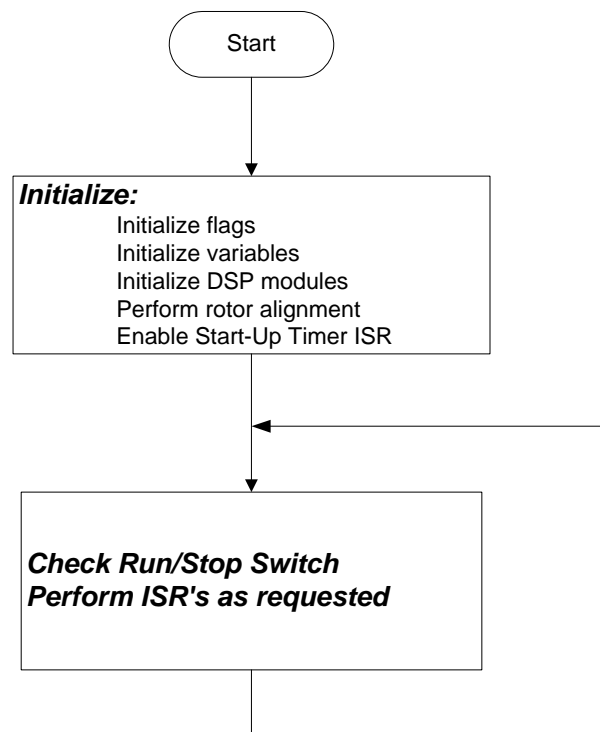


Figure 5.8 : Main program

An ISR can be assigned one of three priority levels. These are 0 (lowest), 1 (normal) and 2 (highest). Subroutines of the same priority are serviced in the order that they are invoked. If a subroutine of higher priority is invoked while another subroutine of lower priority is being serviced, then the latter subroutine is interrupted to allow the former subroutine to be executed. Servicing of the lower priority subroutine is resumed after completion of the higher priority subroutine.

The subroutines forming part of the program are initiated by events such as:

- the timing out of timers;
- the completion of A/D conversion; and
- the loading of the pulse width modulator registers.

5.4.3 The 'Run' state

Four ISRs are executed during the run state. These are:

- the PWM reload ISR (Figure 5.9);
- the ADC complete ISR (Figure 5.11);
- commutation timer (QTC0) OC ISR (Figure 5.15); and
- speed timer (QTC2) OC ISR (Figure 5.18).

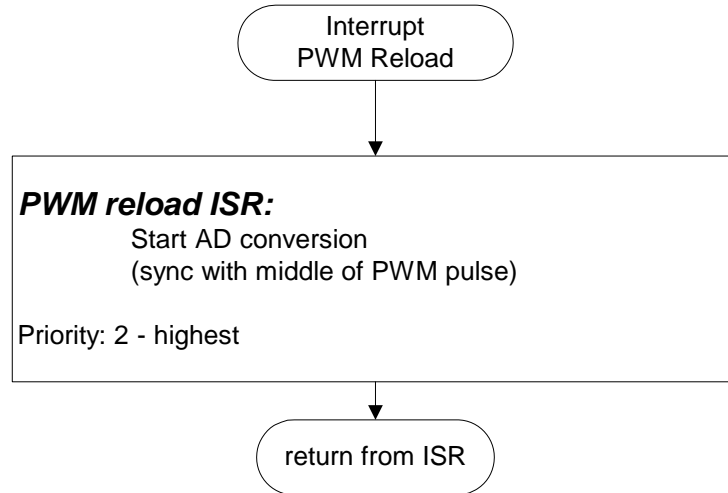
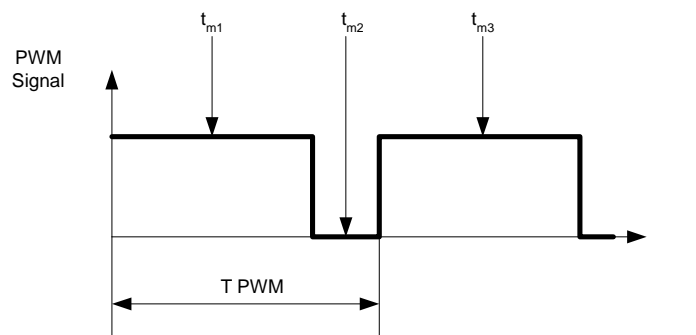


Figure 5.9 : PWM reload ISR

During normal operation the digital signal controller outputs PWM signals based on data loaded in the PWM registers. The data in the PWM register define the PWM duty ratio and the blanking time. Complementary signals are automatically transmitted to the high side and low side power transistors. The ability to mask some of the output channels makes it easy to energise only two phases at a time.



PWM reload ISR initiated at $t_{m1}, t_{m2}, t_{m3}, \dots$

Figure 5.10 : Synchronisation of PWM reload ISR

Figure 5.10 shows the instants at which the PWM reload ISR (Figure 5.9) is invoked. These are synchronized with the middle of PWM pulses. It is during this subroutine that the star-point voltage is measured. The reason for synchronizing the start of the subroutine with the middle of PWM pulses is to avoid the noise generated by switching when the PWM signal changes state. The PWM reload ISR must have high priority because the star-point voltage measurements have to be taken before the PWM signal changes state. Also since the measurements are compared with each other, it is important to take them consistently as close as possible to the middle of the PWM pulses.

The ADC complete ISR (Figure 5.11) is normally executed straight after the PWM reload ISR. Two samples of the star-point voltage are read for each PWM cycle, one sample when the PWM signal is high and one when the PWM signal is low. The difference between those two samples is computed for each PWM cycle. Instead of relying on just the current value of this difference, the program evaluates a running average value of the last few (2-5) calculated differences. This running average value is called SVD in Figure 5.12 and 5.13. Using a running average value improves the system's immunity to noise. In figure 5.12 $SV_{Previous}$ and SV are running average values of the last few (2-5) alternate samples of the star point voltage. If $SV_{Previous}$ is based on samples taken when the PWM signal is high, then SV is based on samples taken when the PWM signal is low. The setting and resetting of the `SkipSample` flag allows separation of the voltage samples needed to update $SV_{Previous}$ from those needed to update SV .

The purpose of the ADC complete ISR is to detect the instant when the equal inductance position is reached and to set the QTC0 timer (counter) at that instant in preparation for the next

commutation. The comparison of SVD with DET_ENABLE (Figures 5.13 and 5.14) is carried out to ensure that once timer QTC0 timer has been prepared for the next commutation, it is not interfered with until that commutation has been carried out. In other words, once equal inductance has been detected the flag DetectionEnable is set to zero and that avoids timer QTC0 timer being further affected by the ADC complete ISR until the next equal inductance position is detected.

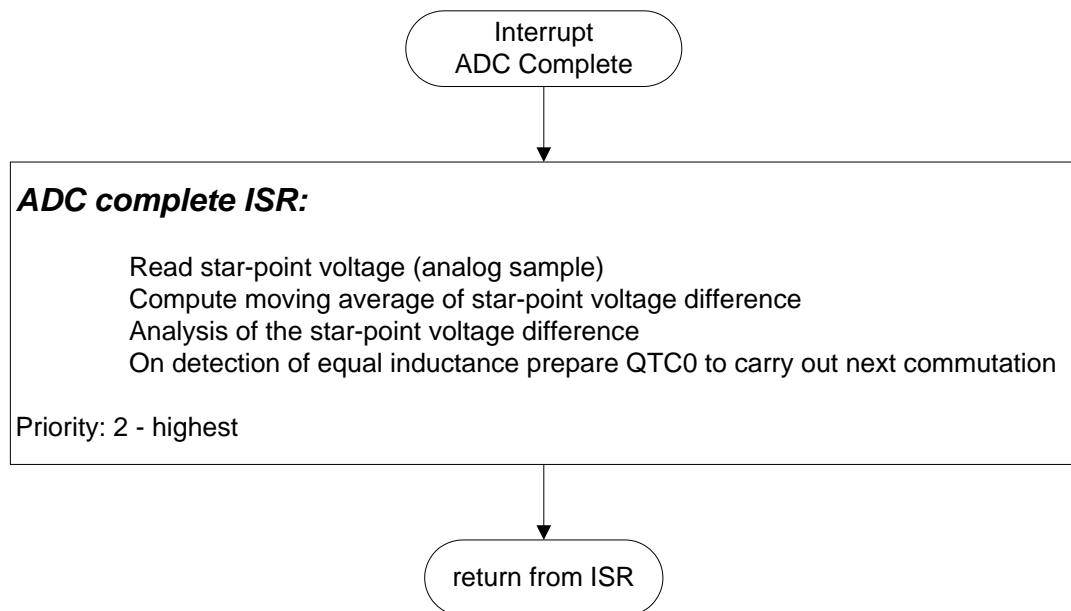


Figure 5.11 : ADC complete ISR

Note that in Figure 5.14 SVD is shown to behave sinusoidally in accordance with equation 4.33.

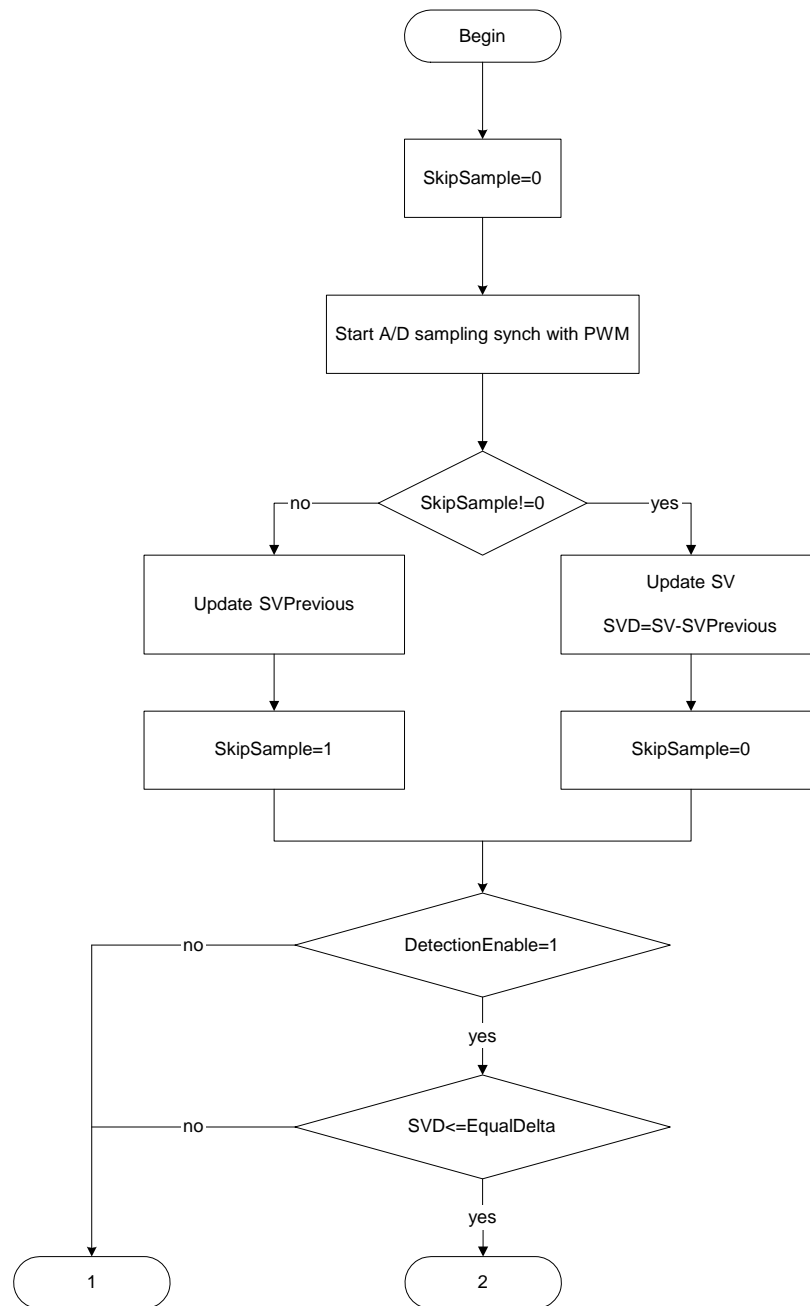


Figure 5.12 : Flow chart for the ADC complete ISR (Part1)

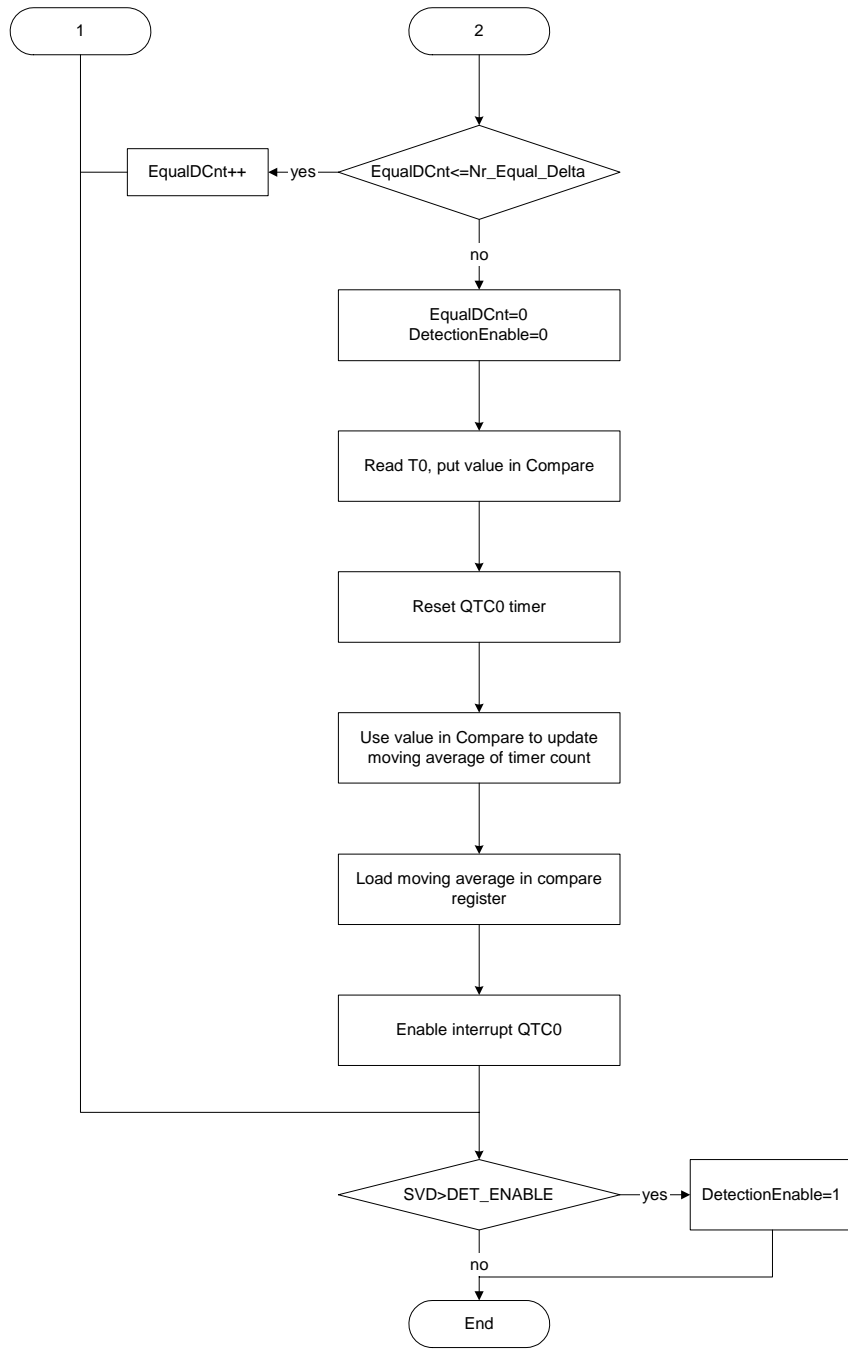


Figure 5.13 : Flow chart for the ADC complete ISR (Part 2)

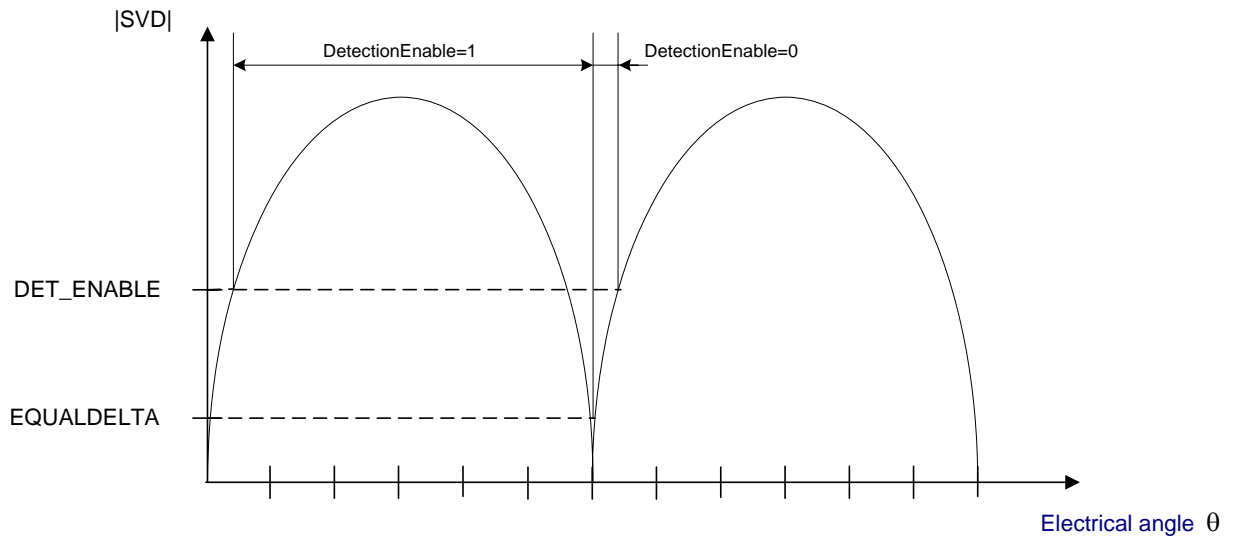


Figure 5.14 : Definition of parameters used in ADC complete ISR

When the absolute value of SVD goes below EQUALDELTA (Figures 5.12 and 5.14) Nr_Equal_Delta times in succession, the equal inductance position is deemed to have been reached. As a result QTC0 timer is read and reset. The value of the QTC0 timer reading (Compare in figure 5.13) is combined with a few (2-5) previous values to form a moving average value which is loaded into the timer compare register. The commutation timer (QTC0) OC ISR (Figure 5.15) is enabled.

For correct operation, the PWM reload ISR and the ADC complete ISR must be completed within a PWM half-cycle. It has been found that in practice, with the DSC that is being used, those two subroutines require a maximum execution time of 6 μ s. With a reasonable PWM frequency of 20kHz, this leaves a minimum of 38 μ s per PWM cycle for the other ISR's. It

should be noted that most of the time the execution times of the ADC complete ISR and the PWM reload ISR add up to less than 6 μ s since |SVD| is normally greater than EQUALDELTA.

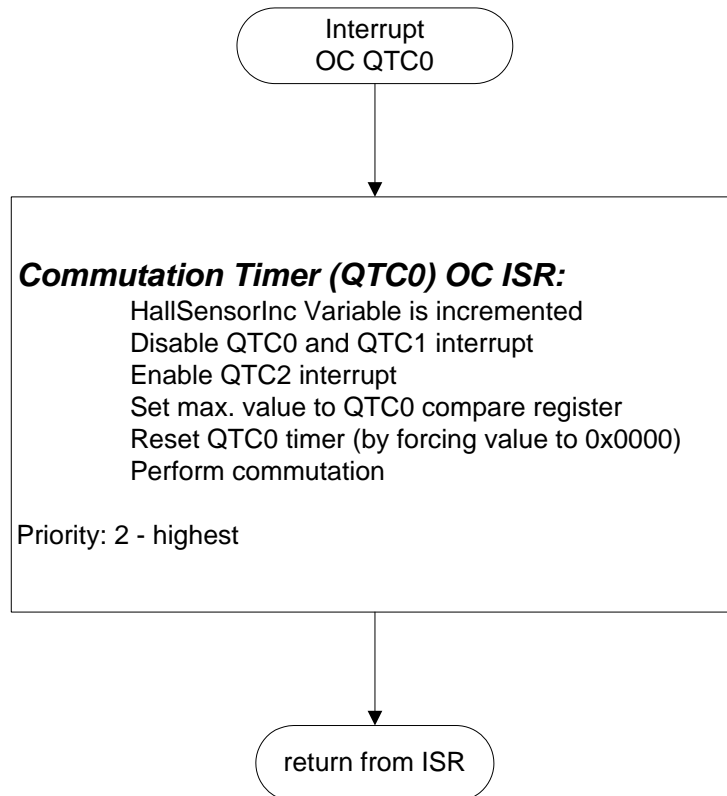


Figure 5.15 : Commutation Timer (QTC0) OC ISR

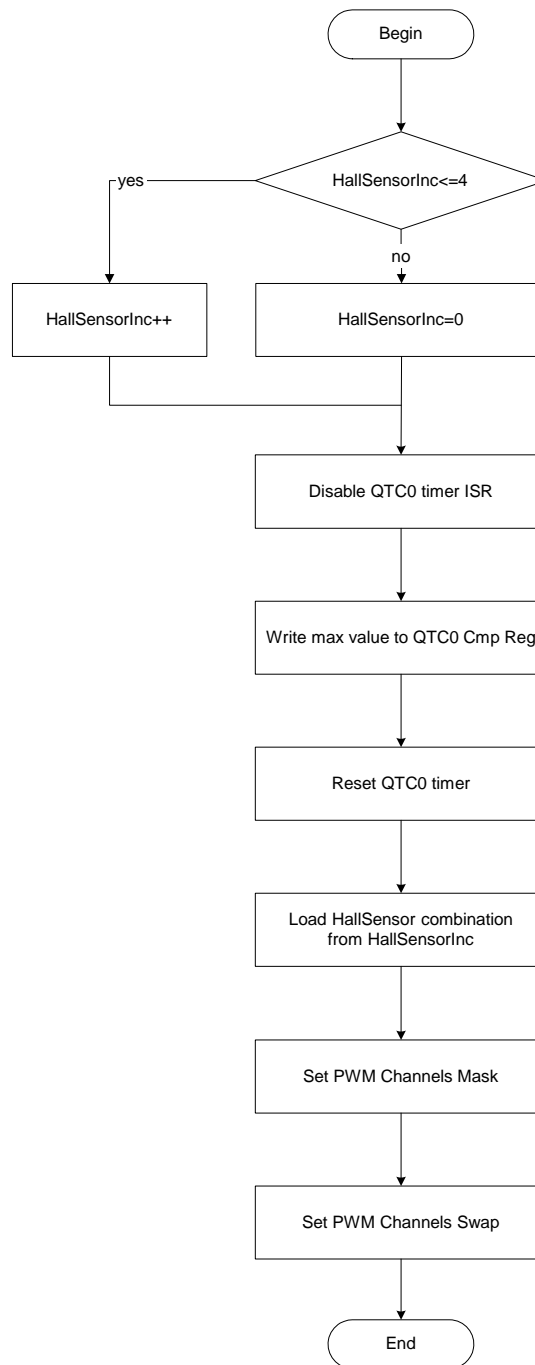
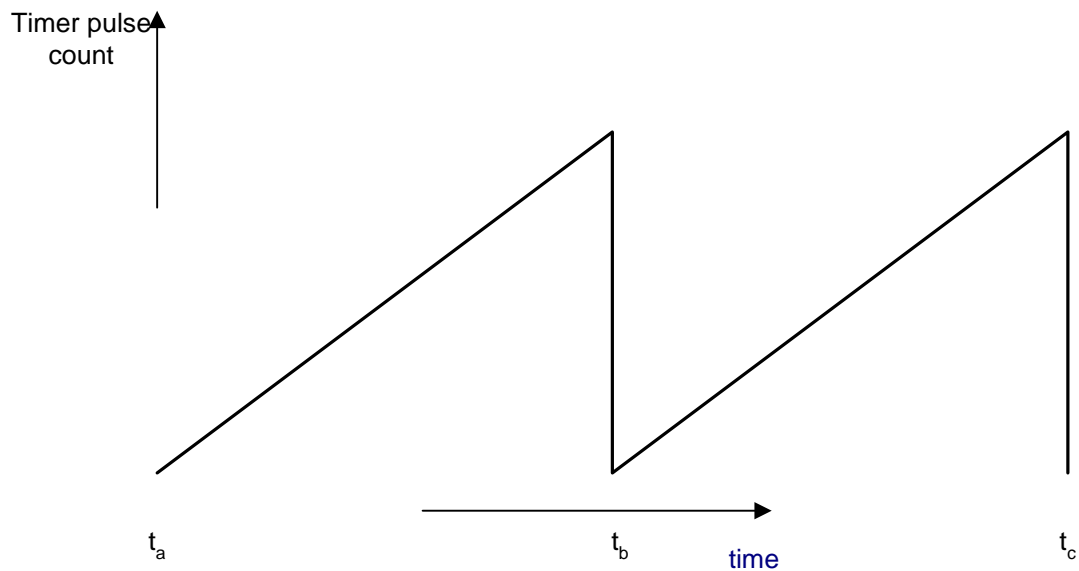


Figure 5.16 : Flow chart for the commutation Timer (QTC0) OC ISR

The purpose of the commutation timer ISR (Figures 5.15 and 5.16) is to execute the next commutation. If it is enabled, the ISR is executed when the timer pulse count (QTC0) becomes equal to the value loaded in the compare register (t_c in Figure 5.17). The value that is loaded in the compare register corresponds to the time interval from the instant the previous commutation was initiated (t_a in Figure 5.17) to the time instant when the most recent equal inductance position was reached (t_b in Figure 5.17). This interval is equivalent to a rotation of 30 electrical degrees. In other words commutation takes place every 60 electrical degrees as required.



At t_b : equal inductance detected; timer compare register loaded; commutation ISR enabled
 At t_a (or t_c): commutation timer ISR initiated; timer QTC0 timer reset; commutation ISR disabled

Figure 5.17 : Timing diagram showing operation of the commutation timer

Variable names (Figure 5.16 and Appendix 1) used in the coding of the commutation timer ISR have been chosen to reflect the close parallel between the equal inductance method and the Hall sensor based method (see Table 1.2). The only significant difference is that in the case of the Hall sensor method commutation instants coincide with the instants the Hall sensor signal vector changes state. In the case of the equal inductance method there exists a thirty degree shift between commutation instants and the instants equal inductance positions are detected.

Once the system is in the run state, the speed timer ISR (figure 5.18) is always enabled. In this version of the program the only purpose of the speed timer ISR is to update the PWM. A PI controller algorithm for the purpose of closed loop speed control can, for example, be fitted into this ISR. At the moment the ISR is initiated every 1 ms. In other versions of the program, this time can be increased or decreased depending on the required execution time.

It should be noted that not all of the 1 ms presently allocated is available to process the code that makes up the ISR. This is because the speed timer ISR has been given lowest priority. Its execution will be continually interrupted by the higher priority ISRs thus reducing the available execution time to below one millisecond.

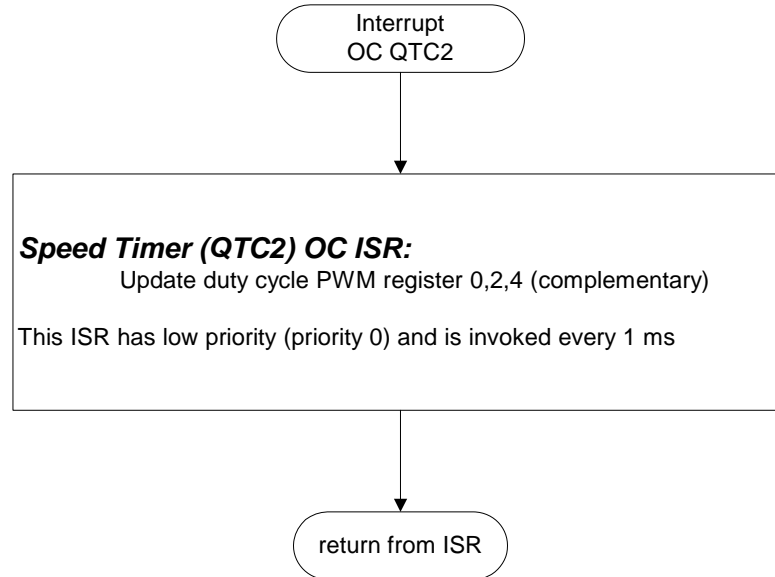


Figure 5.18 : Speed Timer ISR

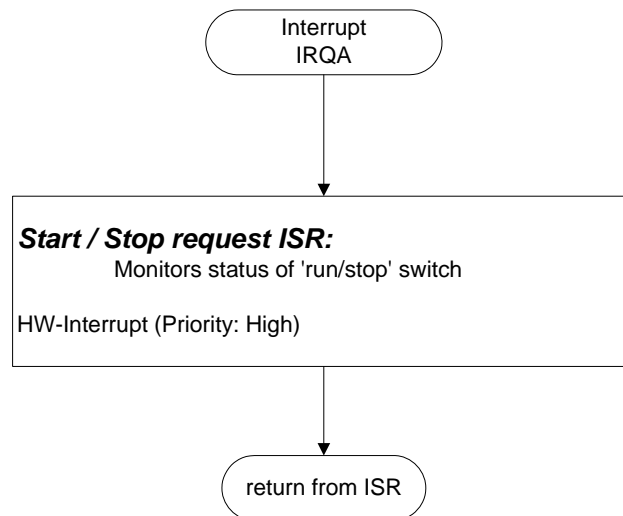


Figure 5.19 : Start/Stop request ISR

The start/stop request ISR (Figure 5.19) is initiated whenever the start/stop switch changes position and the initialization stage is over. If the start/stop switch goes to the stop position, all PWM channels are masked and all other ISRs are disabled. If the start/stop switch changes to the start position, the start-up timer ISR is enabled.

5.4.4 The start-up process

The purpose of the start-up timer ISR (Figure 5.20) is to carry out the first commutation after the rotor has been aligned. Note that the initialization procedure which minimizes back rotation (suggested in Section 4.6) has not been implemented. A simpler start-up process that has been used but there is a 50 percent probability of back rotation which can be up to 180 electrical degrees. Phase pair CA is one of the six possible phase pairs that has been selected for rotor alignment. Note that there is no particular advantage in selecting any other phase pair. Energisation of phase pair CA results in rotor alignment at angle θ_1 (Figure 1.7). The alignment stage is performed during initialization. A quarter of a second after initialization has been carried out the start-up timer ISR is enabled. This is done by resetting timer T1 and loading its timer compare register. As part of the execution of the start-up timer ISR, QTC0 timer is reset. This allows timer QTC0 timer to be used to evaluate the time interval from the instant the first commutation is executed to the instant the equal inductance position is reached. As mentioned before, this information is used by the commutation timer ISR which is executed during the run state. Note that once the run state is entered, the start-up timer ISR is disabled.

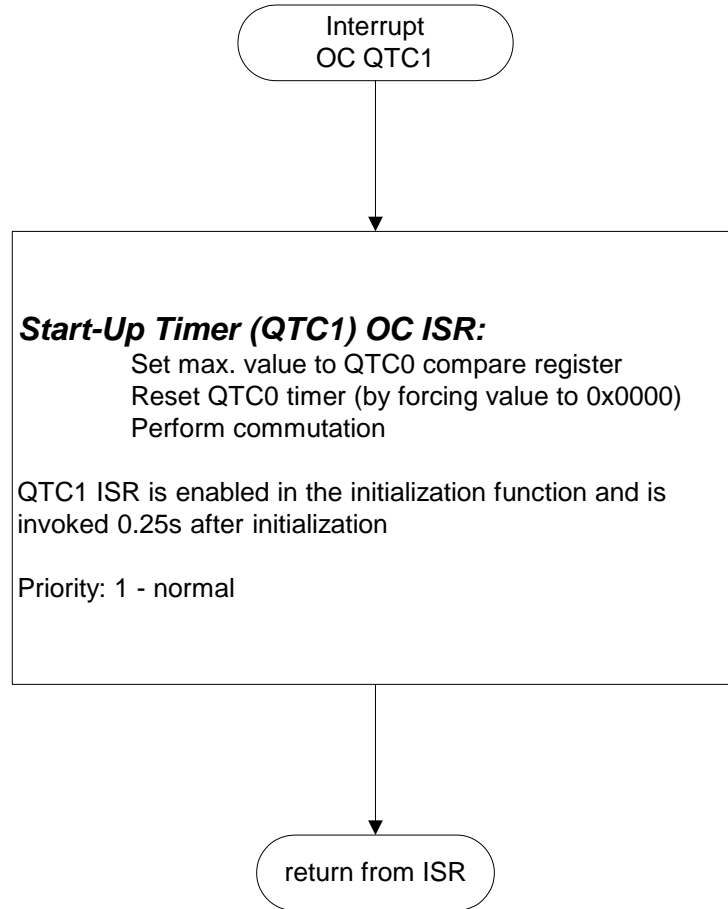


Figure 5.20 : Start-up Timer ISR

5.5 Test Results

A simple way of ascertaining the effectiveness of the equal inductance technique is to compare motor performance when it is used with motor performance when the Hall sensor based method is used. One performance indicator is the current drawn by the motor. Poor commutation results in additional losses which would be reflected in higher current drawn by the motor and lower speed. Table 5.1 shows that speed and current drawn by the motor are practically identical whether the Hall sensor method or the equal inductance method is being used. In addition commutation instants determined by the two methods are compared in Figures 5.21. From Figure 1.6 it can be deduced that a particular transistor will be pulse width modulated continuously for an interval of 120 electrical degrees. From Table 1.2 it can be deduced that a change of state of a particular Hall sensor will initiate that interval if the Hall sensor method is used.

Table 5.1 : Comparison of motor current (dc) and speed for given PWM duty ratios

Duty ratio	60%	65%	70%	75%
Motor Current (mA) Hall sen. method	34	48	81	97
Motor Current (mA) Equal ind. method	35	50	81	99
Speed (Hz) Hall sen. method	11.1	14.5	22.7	27.4
Speed (Hz) Equal Ind. method	11.2	14.6	22.8	27.6

Figures 5.21 show the actual gate signal of the low side A-phase transistor when the equal inductance method is used. There is practically perfect alignment between commutation instants determined by the equal inductance method and the instants the Hall sensor signal changes state. Note that slight misalignments present in Figures 5.21b and 5.21c are most likely due to the oscilloscope's limitations.

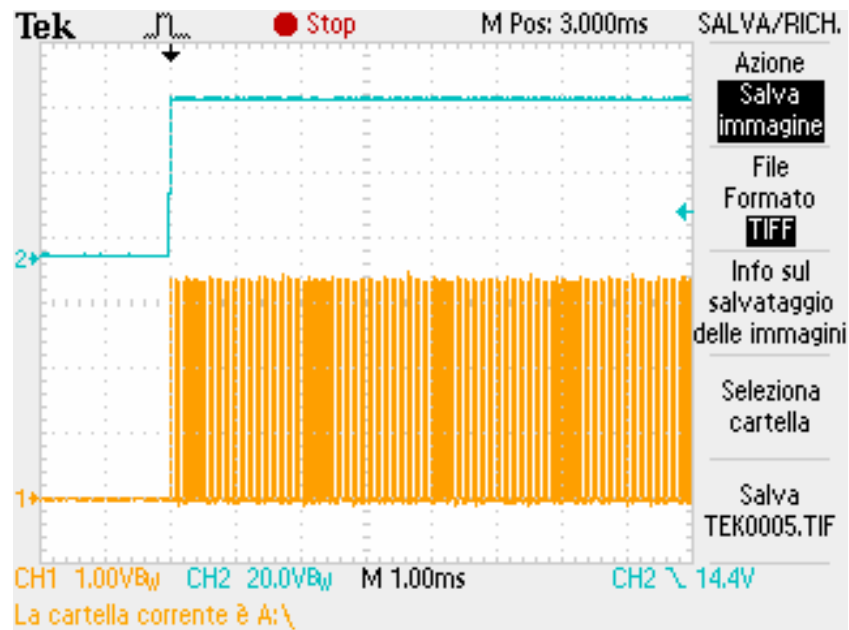


Figure 5.21a : Comparison of the commutation instant (detail)

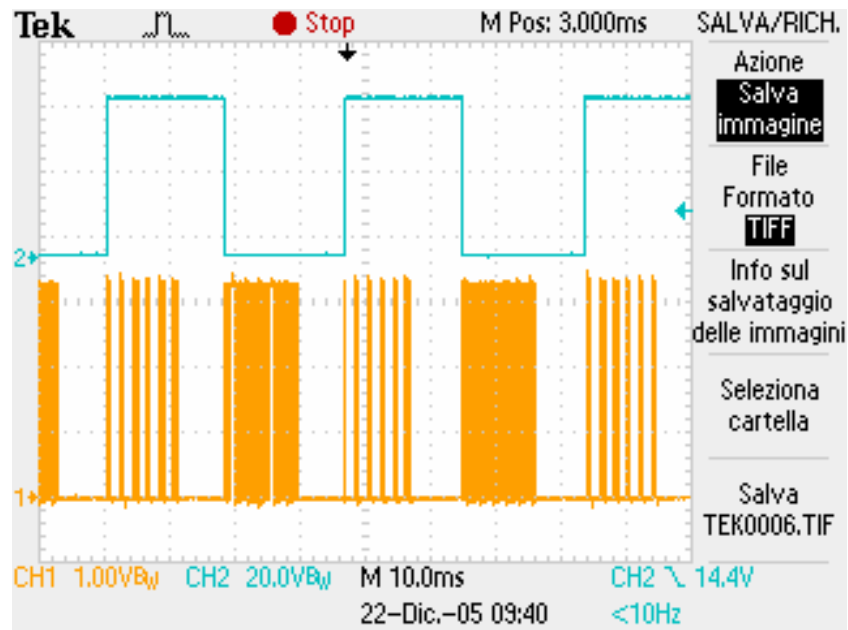


Figure 5.21b : Comparison of the commutation instants (at no load, 100mA)

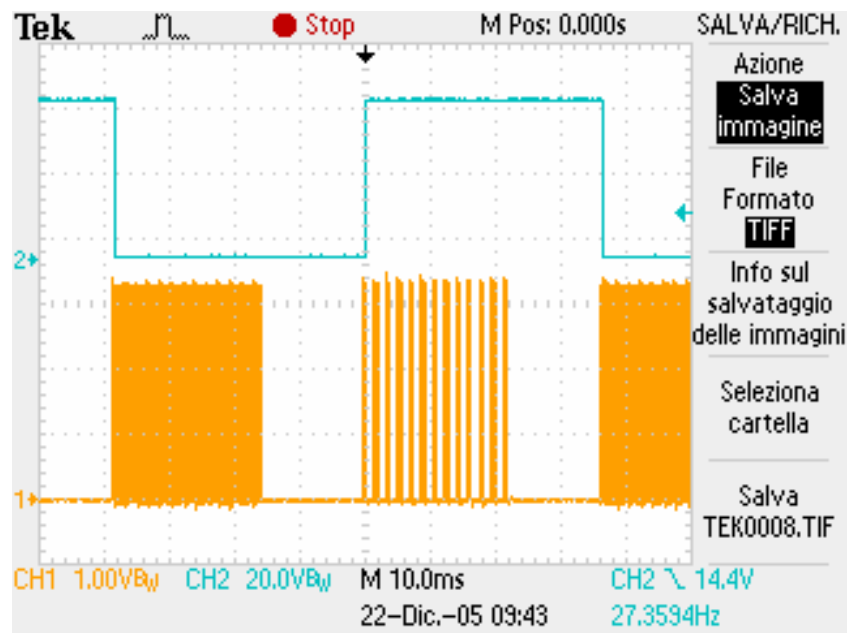


Figure 5.21c : Comparison of the commutation instants (at 500 mA)

Chapter 6

Conclusions

6.1 Theoretical Findings

The aim of this project was the develop a low cost sensorless technique for BLDC motors that offers potential for performance that is equal to or better than that obtained by systems relying on low resolution physical devices such as Hall sensors. After a review of relevant publications, a saliency based method was adopted for the project. The presence of saliency results in variation in the response of machine currents and voltages as a function of rotor position. Rotor position information can be deduced from one or more of those responses. A fundamental question is how to induce those responses. After considering a few options, it was decided to deduce rotor position from the response of the BLDC star-point voltage due to bipolar PWM

voltage pulses that are normally applied to successive phase pairs. Theoretical analysis showed that the star-point voltage is made up of a DC component equal to half the DC supply voltage and an AC component (non-sinusoidal) that is modulated by the rotor movement. In other words the peak to peak value of the AC component varies as rotor position changes. The fundamental frequency of the AC component is equal to the PWM frequency. It was found from the theoretical investigation that a zero peak to peak value of the AC component corresponds to a rotor position that is thirty electrical degrees away from the next ideal commutation position. That rotor position is also the one where the energized phase windings have equal inductances. Hence the adopted sensorless commutation control method was termed the ‘equal inductance method’. Further theoretical analysis showed that the peak to peak value of the AC component of the star-point voltage depends only on the DC supply voltage, the direct axis inductance and the quadrature axis inductance. In other words the position of equal inductance deduced from star-point voltage measurements is insensitive to operational parameters such as load current and circuit parameters such as winding resistance.

BLDC control based on Hall sensors has the advantage of smooth start-up without back rotation. A question relevant to this project was whether or not saliency related measurements could be used to allow smooth starting without back rotation. It has been shown, theoretically, that peak to peak value of the AC component of the star-point voltage is proportional to the difference between the self inductances of the phase pair energized by PWM voltage pulses. Thus by using bipolar PWM pulses with fifty per-cent duty (to avoid rotation) and star-point voltage measurements, the rotor initial position, within a pair of pole pitches, can be narrowed down to within two sixty degree (electrical) ranges. The rotor position can be narrowed down further to a

single sixty degree range by checking whether the difference between the inductances of an appropriately selected phase pair tends to increase or decrease when the pair is energised by means of bipolar PWM pulses with duty cycle gradually changing from fifty per-cent. There is a fifty per-cent probability that checking for this increase or decrease will result in back rotation of up to a few degrees. Once rotor initial position has been narrowed down to within a single sixty degree range, an alignment state follows. After that commutation is based on detected equal inductance positions.

The back EMF method of commutation control relies on detection of zero-crossing instants of the back EMF signal from the unenergised phase. It has been shown that the instant at which the rotor reaches the equal inductance position coincides with the zero-crossing instant of the back EMF of the unenergised phase. There is, therefore, a close parallel between the equal inductance method and the back EMF method. For operation over a wide speed range it may be advantageous to operate using the equal inductance method at low speed and the back EMF method at high speed. The close parallel between the two methods makes it easy to implement changeover strategies from one to the other as the motor speed crosses the chosen boundary between low speed and high speed operation.

In summary the ‘equal inductance method’ was chosen because of:

- ease of implementation requiring relatively little hardware and software resources;

- insensitivity of estimated equal inductance position to operational and circuit parameters;
- the potential for a start-up strategy giving performance almost as good as Hall sensor based systems; and
- the close parallel with the back EMF method allowing easy changeover to that method at high speeds.

6.2 Practical Outcome

The core feature of any system using the equal inductance method would be commutation control based on detection of the instant when the rotor reaches position of equal inductance. Optional features may include, for example, a transfer strategy to and from the back EMF method and closed loop speed control. In this project, however, only the core feature has been implemented. This has required:

- design of a control module including a DSC (digital signal controller) and MOSFET gate drivers;
- design of a MOSFET three-phase inverter bridge; and

- software development for the DSC.

Tests were performed on a BLDC motor that was known to be salient. The saliency ratio (measured at 20 kHz) is around 1.17.

Tests results confirmed that there is practically no difference between commutation instants determined by the equal inductance method and those determined with the help of signals from Hall sensors.

6.3 Further Work

In this project an existing test-motor has been used for practical demonstration of the equal inductance method. It has also been shown that the sensitivity of the method is proportional to the saliency ratio. As expected, a minimum level of saliency is necessary for the equal inductance method to work in practice. This raises questions such as:

- ‘what is the minimum level of saliency needed to guarantee correct operation in practice?’
- ‘what are the consequences of excessive saliency?’

- ‘how can saliency be estimated at the design stage, that is before the BLDC motor is constructed?’

Everyone of the above questions has practical importance and would make good topics for future projects.

Natural extensions of the current project include:

- practical implementation of the suggested start-up process (based on saliency related measurements);
- practical implementation of the strategy allowing switching from the equal inductance method to the back EMF method and vice-versa in applications requiring a relatively wide speed range; and
- modification of the ‘equal inductance method’ aiming to eliminate the need for the star-point connection

Work relating to some of the above points has already started. Preliminary tests have been performed using voltage measurements at the floating terminal rather than the star-point. The results indicate that the ‘Equal Inductance Method’ can work without access to the star-point or even if the windings are delta connected.

References

- Bolognani, S., Oboe, R. & Zigliotto, M. (1999), '*Sensorless full-digital PMSM drive with EKF estimation of speed and rotor position*', IEEE Transaction on Industrial Electronics, Volume 46, Issue 1, pp. 184-191
- Bosch, V. (1997), *Speed controlled single spindle drives for textile machines*, Dissertation, Universität Stuttgart
- Chalupa, L. (2001), *DSP56F80x MC PWM module in motor control applications*, Motorola Literature Distribution, Denver
- Chiricozzi, E., Parasiliti, F., Putrella, R. & Tursini, M (1998), '*Sensorless permanent magnet synchronous motor drive solution for compressor application*', Università di L'Aquila, L'Aquila, Italy; Available at:
http://ww2.polito.it/ricerca/syncrodrive/aquila/Report_Aquila.pdf;
[Accessed 15 Feb 2006]
- Fitzgerald, A., Kingsley, C. & Umans, S. (2003), *Electric machinery*, sixth edn, McGraw Hill, Singapore

- Freescale Semiconductor (2005), *56F8000 16-bit digital signal controller peripheral reference manual*, rev. 0, Freescale Semiconductor Literature Distribution Center, Denver
- Leksell, M., Harnefors, L. & Nee, H. (1998), *Machine design considerations for sensorless control of PM motors*, Royal Institute of Technology, Stockholm; Available at: http://eme.ekc.kth.se/publications/pdf/1998/mats_lennart_hansi_istanbul1998.pdf; [Accessed 15 Feb 2006]
- Kim, S. & Sul, S. (1997), 'New approach for high-performance PMSM drives without rotational position sensors', *IEEE Transaction on Power Electronics*, Volume 12, Issue 5, pp. 904-911
- Kimbark, E. (1955) , '*Power system stability, Volume III, Synchronous Machines*', republished by IEEE Press
- Krishnan, R. (2001), *Electric motor drives: modelling, analysis and control*, Prentice Hall, Upper Saddle River
- Miller, T.J.E. (1989), *Brushless Permanent-Magnet and Reluctance Motor Drives*, Oxford University Press, Oxford
- Ovrebo, S. (2004), *Comparison of excitation signals for low and zero speed estimation of the rotor position in a axial flux PMSM*, NTNU, Trondheim, Norway; Available at: http://www.elkraft.ntnu.no/eno/Papers2002/Sensorless_PMSM_sigurd_ovrebo.pdf; [Accessed 15 Feb 2006]

- Petrovic, V., Stankovic, A. & Blasko, V. (2003), '*Position estimation in salient PM synchronous motors based on PWM excitation transients*', IEEE Transaction on Industry Applications, Volume 39, Issue 3, pp. 835-843
- Prokop, L. (2003), *3-phase BLDC motor control with sensorless back-EMF ADC zero crossing detection using the 56F805, Designer reference manual*, Motorola Czech System Laboratories, Roznov pod Radhostem, Czech Republic
- Robeischl, E. & Schroedl, M. (2004), '*Optimized INFORM measurement sequence for sensorless PM synchronous motor drives with respect to minimum current distortion*', IEEE Transaction on Industry Applications, Volume 40, Issue 2, pp. 591-598
- Schmidt, P., Gasperi, M., Ray, G. & Wijenayake A. (1997), '*Initial rotor angle detection of a non-salient pole permanent magnet synchronous machine*', IEEE Industry Applications Society Annual Meeting, New Orleans
- Sepe, R. & Lang, J. (1992), '*Real-time observer-based (adaptive) control of a permanent magnet synchronous motor without mechanical sensors*', IEEE Transaction on Industry Applications, Volume 28, Issue 6, pp. 1345-1352
- Shouse, K. & Taylor, D. (1998), '*Sensorless velocity control of permanent-magnet synchronous motors*', IEEE Transaction Control System Technology, Volume 6, Issue 3, pp. 313-324
- Stölting, H. & Kallenbach, E. (2002), *Handbuch Elektrische Kleinantriebe*, 2. Auflage, Hanser, Muenchen
- Ueki Y. (1992), '*Detection of relative position between magnetic pole and drive coil in brushless dc motor*', United State Patent, Patent Number 5,159,246

Valentine, R. (1998), *Motor control electronics handbook*, first edn, McGraw Hill, Singapore

Wang, L., Lorenz, R. (2000), '*Rotor Position Estimation for Permanent Magnet Synchronous Motor Using Saliency-Tracking Self-Sensing Method*', In Proc.of IEEE IAS Annual Meeting, Oct. 8-12, Rome, Italy, pp. 445-450

Weiss, W. (1998), '*Artificial heart with sensorless motor*', United State Patent, Patent Number 5,751,125

Appendix A

Firmware

```
/*  
**  
MPhil D.Gambetta  
**/  
  
#include "qs.h"  
  
#include "sys.h"  
#include "intc.h"  
#include "gpio.h"  
#include "adc.h"  
#include "mc.h"  
#include "pwm.h"  
#include "qtimer.h"  
#include "occs.h"  
#include "sci.h"
```

```
#include "freemaster.h"

//Phase Masks
#define PWM_MASK_A      0x0003
#define PWM_MASK_B      0x000C
#define PWM_MASK_C      0x0030

//Defines for Starpoint analysis
static Int16      EQUAL_DELTA;           //Equality range
static Int16      NR_EQUAL_DELTA;       //Number consecutive equal samples
static Int16      NR_DELTA;             //Number of Delta's for average
static Int16      DET_ENABLE;          //Value to re-enable detection

//Duty Cycle
static Int16      Duty;

//Startpoint Analysis
static Int16      SV;
static Int16      SVPrevious;
static Int16      SVD;
static Int16      SVDArr[10];
static Int16      SVDCnt;
static Int16      SkipSample;
static Int16      EqualDCnt;
static Int16      DetectionEnabled;

static Word16     Compare;
static Word16     HallSensorInc;
static UWord16    HallSensorsState;
```

```
static pwm_sChannelControl      PWMState;

static pwm_sComplementaryValues  comp;

static Int16                    CompareCnt;
static Int16                    CmpArr[20];
static Int16                    Cmp;
static Int16                    CmpNum=5;

static Int16                    meanValueCmp;

static Int16                    CommDel;

static void Initialize(void);

static const Word16             HallState[6] = {3,1,5,4,6,2};

//Commutation Table
static const pwm_sChannelControl BLDC_COMMUTATION_TABLE_COMP[8] =
    {{0x003F, 0x0000},
     {PWM_MASK_B, PWM_CHANNEL_01},
     {PWM_MASK_A, PWM_CHANNEL_45},
     {PWM_MASK_C, PWM_CHANNEL_01},
     {PWM_MASK_C, PWM_CHANNEL_23},
     {PWM_MASK_A, PWM_CHANNEL_23},
     {PWM_MASK_B, PWM_CHANNEL_45},
     {0x003F, 0x0000}};
```

```
//Main
int main(void)
{
    archDisableInt();
    Initialize();
    //Loop forever
    while(1)
    {
    }
}

//Initialize
static void Initialize(void)
{
    //Init Variables
    Int16 counter=0;

    //Init Star Point Analysis Variables
    EQUAL_DELTA=40;           //Equality range
    NR_EQUAL_DELTA=1;        //Number consecutive equal samples
    NR_DELTA=3;              //Number of Delta's for average
    DET_ENABLE=100;         //Value to reenable detection

    //Init Duty
    Duty=0x5500;
    CommDel=0;
    //Starpoint voltage analysis
    SV=0;
    SVPrevious=0;
```

```
SVD=0;
SVDCnt=0;
SkipSample=0;
EqualDCnt=0;
DetectionEnabled=1;
meanValueCmp=0;

for (counter=0;counter<=9;counter++)
{
    SVDArr[counter]=0;
}

Compare=0;

// Set Initial Position
HallSensorInc=3;

// configure device pins
ioctl(SYS, SYS_INIT, NULL);
ioctl(GPIO_A, GPIO_INIT, NULL);
ioctl(GPIO_B, GPIO_INIT, NULL);
ioctl(GPIO_C, GPIO_INIT, NULL);

// configure PWM module
ioctl(PWM_A, PWM_INIT, NULL);

// configure AD module
ioctl(ADC, ADC_INIT, NULL);
```

```
// Quad Timer C initialization
ioctl(QTIMER_0, QT_INIT, NULL);
ioctl(QTIMER_1, QT_INIT, NULL);
ioctl(QTIMER_2, QT_INIT, NULL);
ioctl(QTIMER_3, QT_INIT, NULL);

// Disable C0 Compare Interrupt and set compare value
ioctl(QTIMER_0, QT_WRITE_COMPARE_REG1, 0xFFFF);
ioctl(QTIMER_0, QT_INT_DISABLE, QT_COMPARE_INT);

// Disable C1 Compare Interrupt and set compare value
ioctl(QTIMER_1, QT_INT_DISABLE, QT_COMPARE_INT);

// Initialize UART
ioctl(SCI_0, SCI_INIT, NULL);

// FreeMASTER initialization
FMSTR_Init();

//Set Alignment Step based on HallSensorInc
HallSensorsState=HallState[HallSensorInc];

// Calculated new mask for PWM transistors
PWMState = BLDC_COMMUTATION_TABLE_COMP[HallSensorsState];

// Swap phases
ioctl(PWM_A, PWM_SET_SWAP, PWMState.Swap);

// Disable phase
ioctl(PWM_A, PWM_OUTPUT_SOFTWARE_CONTROL, PWMState.Mask);
```

```
comp.pwmChannel_0_Value = Duty;
comp.pwmChannel_2_Value = Duty;
comp.pwmChannel_4_Value = Duty;

// calculates the actual contents of the value registers, fills these registers, sets OK bit
ioctl(PWM_A, PWM_UPDATE_VALUE_REGS_COMPL, &comp);

ioctl(PWM_A, PWM_DEVICE, PWM_ENABLE);

//Increment SensorInc by two (in order to start)
HallSensorInc=HallSensorInc+2;

//Disable C0 Compare Interrupt
ioctl(QTIMER_0, QT_INT_DISABLE, QT_COMPARE_INT);

//Disable C2 Compare Interrupt
ioctl(QTIMER_2, QT_INT_DISABLE, QT_COMPARE_INT);

//Set Counter C1
ioctl(QTIMER_1, QT_WRITE_COMPARE_REG2, 0x0000);
ioctl(QTIMER_1, QT_WRITE_LOAD_REG, 10000);
ioctl(QTIMER_1, QT_WRITE_COUNTER_REG, 10000);
ioctl(QTIMER_1, QT_INT_ENABLE, QT_COMPARE_INT);

// Configure Interrupt Controller (IPR) and enable interrupts
ioctl(INTC, INTC_INIT, NULL);

archEnableInt();
}
```

```
//ISR PWM Reload

#pragma interrupt on
void IsrPWMAReload(void)
{
    // Start new AD conversion
    ioctl(ADC, ADC_START, NULL);

    ioctl(PWM_A, PWM_CLEAR_RELOAD_FLAG, NULL);
}
#pragma interrupt off

//ISR End of Conversion

#pragma interrupt on
void IsrADCAEoC(void)
{
    Int16 temp=0;
    //test
    ioctl(GPIO_B, GPIO_TOGGLE_PIN, BIT_3);

    //Selection of ADC / Channel
    switch (PWMState.Mask)
    {
        case PWM_MASK_A:
        {
            SV=ioctl(ADC, ADC_READ_SAMPLE, 0)>>2;
            break;
        }
    }
}
```

```
    case PWM_MASK_B:
    {
        SV=ioc1(ADC, ADC_READ_SAMPLE, 0)>>2;
        break;
    }
    case PWM_MASK_C:
    {
        SV=ioc1(ADC, ADC_READ_SAMPLE, 0)>>2;
        break;
    }
    default:
        break;
}

if (SkipSample==0)
{
    SVPrevious=SV;
    SkipSample=1;
}
else
{

    //Stack of NR_DELTA Values (new in, oldest out)
    //Shift of 1 index for all values
    //Since NR_DELTA-2 because last ist the new one
    for (SVDCnt=NR_DELTA-1;SVDCnt>=1;SVDCnt--)
    {
        SVDArr[SVDCnt]=SVDArr[SVDCnt-1];
    }
}
```

```
//Index 0 takes the last measured delta
SVDArr[0]=SV-SVPrevious;
temp=0;

//Sum of all Delta's
for (SVDCnt=0;SVDCnt<=NR_DELTA-1;SVDCnt++)
{
    temp=temp+SVDArr[SVDCnt];
}
//Averaging (abs to have only pos values)
SVD=abs(temp)/NR_DELTA;
SkipSample=0;
}
if (DetectionEnabled==1)
{
    if (SVD<=EQUAL_DELTA)
    {
        if (EqualDCnt<=NR_EQUAL_DELTA)
        {
            EqualDCnt++;
        }
        else
        {
            EqualDCnt=0;
            DetectionEnabled=0;
            Compare=ioctl(QTIMER_0,QT_READ_COUNTER_REG,
            NULL);

            //Set Counter Register to 0
        }
    }
}
```

```
ioctl(QTIMER_0, QT_WRITE_COUNTER_REG, 0x0000);

for (CompareCnt=CmpNum-1;CompareCnt>=1;CompareCnt--)
{
    CmpArr[CompareCnt]=CmpArr[CompareCnt-1];
}
//Index 0 takes the last measured delta
CmpArr[0]=Compare/20;
meanValueCmp=0;

//Sum of all Delta's
for(CompareCnt=0;CompareCnt<=CmpNum 1;CompareCnt++)
{
    meanValueCmp=meanValueCmp+CmpArr[CompareCnt];
}

//Calculate moving average
Cmp=meanValueCmp/CmpNum*20;

//Set New Compare1 Register
ioctl(QTIMER_0,QT_WRITE_COMPARE_REG1,
Cmp+CommDel);

//Enable Interrupt
ioctl(QTIMER_0, QT_INT_ENABLE, QT_COMPARE_INT);
    }
}
}

if (abs(SVD)>=DET_ENABLE) DetectionEnabled=1;
```

```
//test
ioctl(GPIO_B, GPIO_TOGGLE_PIN, BIT_3);
ioctl(ADC, ADC_CLEAR_STATUS_EOSI, NULL);
}
#pragma interrupt off

//ISR QT0

#pragma interrupt on
void IsrQT0(void)
{
    if (HallSensorInc<=4)
        HallSensorInc=HallSensorInc+1;
    else
        HallSensorInc=0;

    //Disable C0 Compare Interrupt
    ioctl(QTIMER_0, QT_INT_DISABLE, QT_COMPARE_INT);

    //Disable C1 Compare Interrupt (once disabled)
    ioctl(QTIMER_1, QT_INT_DISABLE, QT_COMPARE_INT);

    //Enable C2 Compare Interrupt (once enabled)
    ioctl(QTIMER_2, QT_INT_ENABLE, QT_COMPARE_INT);

    //Set New Compare1 Register
    ioctl(QTIMER_0, QT_WRITE_COMPARE_REG1, 0xFFFF);
```

```
//Set Counter Register to 0
ioctl(QTIMER_0, QT_WRITE_COUNTER_REG, 0x0000);

//Virtual Hallsensor state
HallSensorsState=HallState[HallSensorInc];

// Calculated new mask for PWM transistors
PWMState = BLDC_COMMUTATION_TABLE_COMP[HallSensorsState];

// Swap phases
ioctl(PWM_A, PWM_SET_SWAP, PWMState.Swap);

// Disable phase
ioctl(PWM_A, PWM_OUTPUT_SOFTWARE_CONTROL, PWMState.Mask);

//clears the interrupt flag
ioctl(QTIMER_0, QT_CLEAR_FLAG, QT_COMPARE_FLAG);
}
#pragma interrupt off

//ISR QT1

#pragma interrupt on
void IsrQT1(void)
{

//Set New Compare1 Register
ioctl(QTIMER_0, QT_WRITE_COMPARE_REG1, 0xFFFF);
```

```
//Set Counter Register to 0
    ioctl(QTIMER_0, QT_WRITE_COUNTER_REG, 0x0000);

    //Virtual Hallsensor state
    HallSensorsState=HallState[HallSensorInc];

    // Calculated new mask for PWM transistors
    PWMState = BLDC_COMMUTATION_TABLE_COMP[HallSensorsState];

    // Swap phases
    ioctl(PWM_A, PWM_SET_SWAP, PWMState.Swap);

    // Disable phase
    ioctl(PWM_A, PWM_OUTPUT_SOFTWARE_CONTROL, PWMState.Mask);

    //clears the interrupt flag
    ioctl(QTIMER_1, QT_CLEAR_FLAG, QT_COMPARE_FLAG);
}
#pragma interrupt off
```

```
//ISR QT2

#pragma interrupt on
void IsrQT2(void)
{

    // sets 50% duty cycle for all channels
    comp.pwmChannel_0_Value = Duty;
    comp.pwmChannel_2_Value = Duty;
    comp.pwmChannel_4_Value = Duty;

    // calculates the actual contents of the value registers, fills these registers, sets OK bit
    ioctl(PWM_A, PWM_UPDATE_VALUE_REGS_COMPL, &comp);

    // clears the interrupt flag
    ioctl(QTIMER_2, QT_CLEAR_FLAG, QT_COMPARE_FLAG);

    FMSTR_Poll();
}
#pragma interrupt off
```